
Recurrent Ladder Networks

Alexander Ilin, Isabeau Prémont-Schwarz, Tele Hotloo Hao
Antti Rasmus, Rinu Boney, Harri Valpola
The Curious AI Company
{alexilin,isabeau,hotloo,antti,rinu,harri}@cai.fi

Abstract

We propose a recurrent extension of the Ladder network [24], which is motivated by the inference required in hierarchical latent variable models. We demonstrate that the recurrent Ladder is able to handle a wide variety of complex learning tasks that benefit from iterative inference and temporal modeling. The architecture shows close-to-optimal results on temporal modeling of video data, competitive results on music modeling, and improved perceptual grouping based on higher order abstractions, such as stochastic textures and motion cues. We present results for fully supervised, semi-supervised, and unsupervised tasks. The results suggest that the proposed architecture and principles are powerful tools for learning a hierarchy of abstractions, handling temporal information, modeling relations and interactions between objects.

1 Introduction

Many cognitive tasks require learning useful representations on multiple abstraction levels. Hierarchical latent variable models are an appealing approach for learning a hierarchy of abstractions. The classical way of learning such models is by postulating an explicit parametric model for the distributions of random variables. The inference procedure, which evaluates the posterior distribution of the unknown variables, is then derived from the model—an approach adopted in probabilistic graphical models (see, e.g., [3]).

The success of deep learning can, however, be explained by the fact that popular deep models focus on learning the inference procedure directly. For example, a deep classifier like AlexNet [20] is trained to produce the posterior probability of the label for a given data sample. The representations that the network computes at different layers are related to the inference in an implicit latent variable model but the designer of the model does not need to know about them.

However, it is actually tremendously valuable to understand what kind of inference is required by different types of probabilistic models in order to design an efficient network architecture. Ladder networks [24, 29] are motivated by the inference required in a hierarchical latent variable model. By design, the Ladder aims to emulate a message passing algorithm, which includes a bottom-up pass (from input to label in classification tasks) and a top-down pass of information (from label to input). The results of the bottom-up and top-down computations are combined in a carefully selected manner.

The original Ladder network implements only one iteration of the inference algorithm but complex models are likely to require iterative inference. In this paper, we propose a recurrent extension of the Ladder network for iterative inference and show that the same architecture can be used for temporal modeling. We also show how to use the proposed architecture as an inference block in more complex models which can handle multiple independent objects in the sensory input. Thus, the proposed architecture is suitable for the type of inference required by rich models: those that can learn a hierarchy of abstractions, can handle temporal information and can model multiple objects in the input. We demonstrate that the recurrent Ladder is able to handle a wide variety of complex

learning tasks: It shows close-to-optimal results on temporal modeling of video data, competitive results on music modeling, and improved perceptual grouping based on higher order abstractions, such as natural textures and motion cues.

2 Recurrent Ladder

The structure of the Ladder networks is motivated by emulating a message-passing algorithm in hierarchical latent variable models (HLVM). In this section, we illustrate this by deriving inference algorithms for simple HLVMs, discussing the connection to message passing and showing that the inference procedure can be implemented using the Ladder computational graph. We also present a recurrent extension of the Ladder networks and show that it can emulate both iterative inference and state estimation in temporal models. We also review a previously developed model for perceptual grouping (Tagger, [12]) from the perspective of iterative inference in a probabilistic model and motivate using the proposed recurrent Ladder as a building block in Tagger.

2.1 The Ladder family of architectures

In this article we consider the class of (recurrent) models which consist of an encoder, which takes in the input and outputs a high-level representation, and a decoder, which takes in a high-level representation and outputs a vector in the input space¹. At each recursion instance $t \in \{1, \dots, T\}$, calculations proceed from the input up through the encoder and the back down the decoder. In what follows of this section, we will use Greek letters to denote functions and Latin letters to denote vectors of activations. At each level $l \in \{1, \dots, L\}$ of there is an encoder function κ_l ² and a decoder function α_l ³.

The output of κ_l at iteration t is a 3-tuple denoted $(v_{l,t}^e, h_{l,t}^e, s_{l,t}^e)$, where $v_{l,t}^e$ is to be passed vertically up the encoder to κ_{l+1} at iteration t , $h_{l,t}^e$ is to be passed horizontally to the next decoder pass (i.e. to the decoder at iteration t), and $s_{l,t}^e$ is an internal state for the layer (in case it is different from v or h). Similarly for the decoder, the output of α_l at iteration t is a 3-tuple denoted $(v_{l,t}^d, h_{l,t}^d, s_{l,t}^d)$, where $v_{l,t}^d$ is to be passed vertically down the decoder to α_{l-1} at iteration t , $h_{l,t}^d$ is to be passed horizontally to the next encoder pass (i.e. to the encoder at iteration $t+1$), and $s_{l,t}^d$ is an internal state for the layer (in case it is different from v or h).

We identify the input x_t with $v_{0,t}^e$. In the stateless case, s will simply be set to zero.

The input to κ_l at iteration t is the tuple $(v_{l-1,t}^e, s_{l,t-1}^e, i_{l,t}^e)$ where $i_{l,t}^e$ is the input from the decoder at the last iteration and is $\{h_{l-j,t-1}^d\}_{j \in \Lambda^{d \rightarrow e}}$, where $\Lambda^{d \rightarrow e} \subset \{-1, 0, +1\}$ is the possibly empty set which describes which decoder to encoder connections there are, and which does not depend on either l or t . $\Lambda^{d \rightarrow e}$ determines the routing between the decoder and the next encoder: if 0 is in $\Lambda^{d \rightarrow e}$, this means that the encoder at level l gets a input the lateral output of the previous decoder at level l , while if ± 1 is in $\Lambda^{d \rightarrow e}$, this means that the encoder at level l gets a input the lateral output of the previous decoder at level $l \pm 1$. Similarly, for the decoder we have that the input to α_l at iteration t is the tuple $(v_{l+1,t}^d, s_{l,t-1}^d, i_{l,t}^d)$ where $i_{l,t}^d$ is the input from the encoder at the current iteration and is $\{h_{l-j,t}^e\}_{j \in \Lambda^{e \rightarrow d}}$, where $\Lambda^{e \rightarrow d} \subset \{-1, 0, +1\}$ describes which lateral (encoder to decoder) connections there are, and does not depend on either l or t . Furthermore we identify the vertical output of the last layer of the encoder with the vertical input of the last layer of the decoder, $v_{L+1,t}^d := v_{L,t}^e$.

¹Or a space sufficiently close to the input space. Like for example, in the case of image input space, a heat map over the input image, or a labeling of each pixel of the image.

²For the first letter of κωδικοποιώ, the Greek verbe for “to encode”.

³For the first letter of αποκωδικοποιώ, the Greek verbe for “to decode”.

In summary, we consider the class of neural networks which are functionally of the following form. The encoder is, $\forall t \in \{1, \dots, T\}$ and $\forall l \in \{1, \dots, L\}$:

$$v_{0,t}^e := x_t, \quad (1)$$

$$\Lambda^{d \rightarrow e} \subset \{-1, 0, +1\}, \quad (2)$$

$$i_{l,t}^e := \{h_{l-j,t-1}^d\}_{j \in \Lambda^{d \rightarrow e}}, \quad (3)$$

$$(v_{l,t}^e, h_{l,t}^e, s_{l,t}^e) = \kappa_l(v_{l-1,t}^e, s_{l,t-1}^e, i_{l,t}^e). \quad (4)$$

The decoder is, $\forall t \in \{1, \dots, T\}$ and $\forall l \in \{1, \dots, L\}$:

$$v_{L+1,t}^d := v_{L,t}^e, \quad (5)$$

$$\Lambda^{e \rightarrow d} \subset \{-1, 0, +1\}, \quad (6)$$

$$i_{l,t}^d = \{h_{l-j,t}^e\}_{j \in \Lambda^{e \rightarrow d}}, \quad (7)$$

$$(v_{l,t}^d, h_{l,t}^d, s_{l,t}^d) = \alpha_l(v_{l+1,t}^d, s_{l,t-1}^d, i_{l,t}^d). \quad (8)$$

In what follows, we will formulate concrete realizations of the using only $\Lambda^{d \rightarrow e} = \Lambda^{e \rightarrow d} = \{0\}$ by using specially chosen differences in the lateral and vertical outputs. In the case of iterative inference however, it would have been possible to achieve the message passing by having the lateral and vertical outputs being equal, and having $\Lambda^{d \rightarrow e} = \{0, +1\}$, $\Lambda^{e \rightarrow d} = \{-1, 0\}$. We have not yet tested this variant empirically.

2.2 Ladder learns an inference procedure

The original Ladder networks [24] emulate an inference procedure for a static HLVM. The networks are usually trained with an auxiliary (denoising) task which encourages the network to learn the inference procedure. In this subsection, we derive an inference procedure for an explicit HLVM and show that the denoising algorithm justifies the structure of the computational graph of the original Ladder networks.

We consider a probabilistic model with three one-dimensional variables whose joint probability distribution is given by

$$p(x, y, z) = p(z)p(y|z)p(x|y) \quad (9)$$

$$p(x|y) = N(x|w_x y, \sigma_x^2) \quad (10)$$

$$p(y|z) = N(y|w_y z, \sigma_y^2) \quad (11)$$

$$p(z) = N(z|\mu_z, \sigma_z^2), \quad (12)$$

where $N(\cdot|m, v)$ denotes the Gaussian probability density function with mean m and variance v . We want to derive a denoising algorithm that recovers clean observation x from its corrupted version \tilde{x} , where the corruption is also modeled to be Gaussian:

$$p(\tilde{x}|x) = N(\tilde{x}|x, \sigma^2). \quad (13)$$

This gives the graphical representation of the model shown in Fig. 1a. The reason we look at denoising, is because it is a task which implements unsupervised learning of the data distribution [1]⁴.

In order to do optimal denoising, one needs to evaluate the expectation of $p(x|\tilde{x})$, which can be done by learning the joint posterior distribution of the unknown variables x, y and z . For this linear Gaussian model, it is possible to derive an inference algorithm that is guaranteed to produce the exact posterior distribution in a finite number of steps (see, e.g., [3]). The optimal algorithm propagates messages between the nodes of the graph in Fig. 1a, and only two passes of message propagation (bottom-up and top-down) are needed. However, in more complex models, the posterior distribution of the latent variables is impossible to represent exactly and therefore a neural network that learns the inference procedure needs to represent an approximate distribution. To this end, we derive an approximate inference procedure for this simple probabilistic model.

⁴See <https://thecuriousai.com/blog-part-1/> for a discussion.

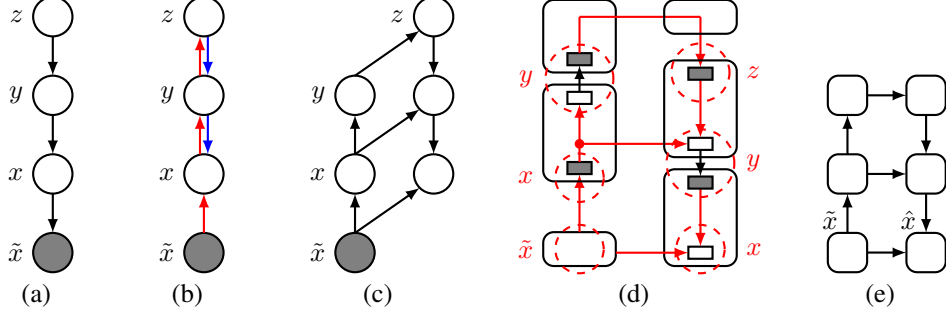


Figure 1: (a): Simple static hierarchical latent variable model. (b): Directions of message propagation. (c): Computational graph implementing message propagation in (b). (d): The structure of the Ladder network can be seen as a computational graph implementing message propagation in (c). The red circles mark the operations corresponding to the nodes of the graph in (b). (d): The structure of the recurrent Ladder (RLadder) network.

Using, for example, the variational Bayesian approach [21], we can approximate the joint posterior distribution with a distribution of a simple form. For example, all the latent variables can be modeled to be independent Gaussian variables a posteriori:

$$p(x, y, z|\tilde{x}) \approx q(x, y, z) = q(x)q(y)q(z), \quad (14)$$

$$q(x) = N(x|m_x, v_x), \quad (15)$$

$$q(y) = N(y|m_y, v_y), \quad (16)$$

$$q(z) = N(z|m_z, v_z). \quad (17)$$

The task is then to find the values of the m and v variables which provide the best approximation. The optimal posterior approximation is found by minimizing the lower bound of the Kullback-Leibler divergence between the true distribution and the approximation:

$$C_{\text{VB}} = \int \log \frac{q(x)q(y)q(z)}{p(y, z, \tilde{x})} q(x)q(y)q(z) dydz = \langle \log q(x)q(y)q(z) \rangle - \langle \log p(x, y, z, \tilde{x}) \rangle \quad (18)$$

where $\langle \cdot \rangle$ denotes the expectation over $q(x, y, z)$. Note that we derive an inference procedure which estimates parameters $m_x, v_x, m_y, v_y, m_z, v_z$ of the approximate posterior (14)–(17) for the model in (9)–(13) with fixed parameters $w_x, \sigma_x^2, w_{yz}, \sigma_y^2, \mu_z, \sigma_z^2, \sigma^2$.

In Appendix A, we derive the learning rules for the variational parameters in approximation (14)–(17). For example, the mean parameters can be updated using the following rules:

$$m_x = s_x \tilde{x} + (1 - s_x) w_y m_y \quad (19)$$

$$m_y = s_y \frac{m_x}{w_x} + (1 - s_y) w_{yz} m_z \quad (20)$$

$$m_z = s_z \frac{m_y}{w_{yz}} + (1 - s_z) \mu_z \quad (21)$$

where

$$s_x = \text{sigmoid}(\log(\sigma_x^2/\sigma^2)) \quad (22)$$

$$s_y = \text{sigmoid}(\log(\sigma_y^2 w_x^2/\sigma_x^2)) \quad (23)$$

$$s_z = \text{sigmoid}(\log(\sigma_z^2 w_{yz}^2/\sigma_y^2)). \quad (24)$$

Thus, in order to update parameters corresponding to y , one needs information from below (e.g., m_x/w_x and w_x^2/σ_x^2) and from above (e.g., $w_{yz}m_z, 1/\sigma_y^2$). Similarly, the computations for x require the information from below (e.g., \tilde{x} and $1/\sigma^2$) and from above (e.g., $w_y m_y, 1/\sigma_x^2$). We can think of the information needed for updating the parameters describing the posterior distributions of the latent variables as ‘messages’ propagating between the nodes of a probabilistic graphical model. Fig. 1b shows the flow of information needed to update the variational parameters. Note that there are mutual dependencies between m_x, m_y and m_z in (19)–(21), which means that the update rules need to be

iterated multiple times until convergence. One iteration of this procedure can be implemented using a computational graph with one bottom-up and one-top down pass, as shown in Fig. 1c.

One implementation of a neural network which can implement a one pass version of Eqs. (19)-(24) is using Eqs. (1)-(8) with $T = 1$ (thus we can disregard the t indices), and

$$\Lambda^{d \rightarrow e} = \emptyset, \quad (25)$$

$$e_l = \tau_l(v_{l-1}^e), \quad (26)$$

$$v_l^e = \rho_l(e_l), \quad (27)$$

$$h_l^e = e_l, \quad (28)$$

$$s_l^e = 0, \quad (29)$$

for the encoder, where τ_l is an affine transformation (for example a fully connected layer, a convolutional layer, or a transposed convolution layer), and ρ_l is a pointwise activation function (typically non-linear like a ReLu or tanh). And in addition having

$$\Lambda^{e \rightarrow d} = \{0\}, \quad (30)$$

$$h_l^d = 0, \quad (31)$$

$$s_l^d = 0, \quad (32)$$

and where α_l implements a multiplicative gating between projections of v_{l-1}^d and h_l^e . These are the equations for the original Ladder paper [24].

Ladder networks have the same structure as the computational graph but the nodes of the Ladder graph do not necessarily correspond to the nodes of a graphical model. As shown in Fig. 1d, some nodes of the Ladder networks consists of two operations, where the first one changes the dimensionality of the input signal and the second does not. The message-passing structure from Fig. 1c can be observed in the Ladder graph by re-grouping the operations as shown with the red circles in Fig. 1d. Fig. 1e shows the usual presentation of the Ladder network structure. Note that the computations proposed for the decoder (top-down pass) of the Ladder networks [24] are justified by the gating structure of the update rules (19)–(24).

The inference procedure can be built around optimizing the cost function in (18) in the case the probabilistic model is explicitly defined as in (9)–(13). This is done, for example, in variational auto-encoders (VAE) [19]. In Ladder networks, the cost function is often formulated around the denoising task:

$$C_{\text{den}} = (x - \hat{x})^2 \quad (33)$$

where the optimal denoising requires inference in an *implicitly* defined probabilistic model. In the considered explicit probabilistic model, the optimal reconstruction \hat{x} using the posterior approximation (14)–(17) is given by m_{x^*} , the estimation of which requires the inference procedure.

To summarize, encouraged by the low-level denoising cost, Ladder networks learn to do inference for an implicitly assumed probabilistic model. The structure of the Ladder computational graph mimics the structure of the message-passing inference procedure that can be derived for an explicit probabilistic model with a chain structure. One advantage of not having to specify the probabilistic model explicitly is that the Ladder network is not restricted to learn inference in a directed graphical model (like in VAE) but can learn inference for an undirected model too. Chain-shaped undirected graphical models have the same kind of message-passing structure during inference and therefore can also be handled by the Ladder computational graph.

2.3 Iterative inference with Ladder

The Ladder learns to amortize the inference, that is it tries to find the best possible solution after one iteration of the bottom-up and top-down updates. However, in complex cognitive tasks it can be difficult to provide an accurate solution after just one bottom-up and top-down iteration. Suppose the task is to recognize a textured digit on a textured background, as shown in the top row of Fig. 8. There, in order to classify a digit, one needs to understand the boundaries between the object and the background, which requires understanding the textures, which in turn can be accurately modeled when the object is well separated. It is also known that the optimal inference in a chain-shaped graphical model can be done in one bottom-up and top-down iteration only for simple (linear Gaussian) models

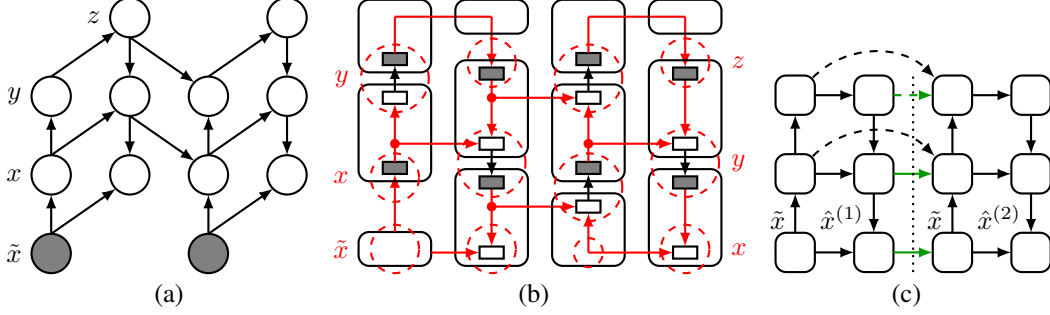


Figure 2: (a): The computational graph iterating message propagation in a graphical model from Fig. 1a. (b): The structure of the recurrent Ladder network can be seen as a computational graph implementing message propagation in (b). The red circles mark the operations corresponding to the nodes of the graph in (c). (c) The structure of the recurrent Ladder for iterative inference.

(see, e.g., [3]). For more complex models, one typically needs an inference procedure that iteratively improves the approximation of the posterior distribution (see, e.g., [31, 22]). Even for the simple model considered in the previous section, one needs an iterative procedure (19)–(24) to find the best *approximation* of the posterior distribution.

An inference algorithm which combines bottom-up and top-down messages on different levels can be implemented by a computational graph in Fig. 2a. The same structure can be implemented by multiple copies of the Ladder network with shared weights as shown in Fig. 2b-c. Because of the recurrent connections we call this architecture Recurrent Ladder (RLadder). As suggested by (19)–(24), in the bottom-up pass of a new iteration one should have access to the latest estimates of the parameters describing the variables from one level above, which justifies the decoder-to-encoder connections shown with the green arrows in Fig. 2c. In practice, we also use skip connections (dashed links in Fig. 2a) to facilitate training of a deep network.

To solve of the form of Eqs. (19)–(24) iteratively, we may simply add a state s to be modified iteratively, but more importantly, give the most up to date top down message to the encoder (from the decoder). This means modifying Eqs. (25)–(32) as follows (this time with $T > 1$):

$$\Lambda^{d \rightarrow e} = \{0\}, \quad (34)$$

$$g_t^{e_i} = \sigma(\tau_l^{e_{1,i}}(v_{l-1,t}^e) + \tau_l^{e_{2,i}}(h_{l,t-1}^d) + \tau_l^{e_{3,i}}(s_{l,t-1}^e)), \forall i \in \{1, 2, 3\}, \quad (35)$$

$$e_{l,t} = g_t^{e_1} \cdot \tau_l^{e_1}(v_{l-1,t}^e) + g_t^{e_2} \cdot \tau_l^{e_2}(h_{l,t-1}^d) + g_t^{e_3} \cdot \tau_l^{e_3}(s_{l,t-1}^e), \quad (36)$$

$$v_l^e = \rho_l^e(e_{l,t}), \quad (37)$$

$$h_l^e = e_{l,t}, \quad (38)$$

$$\Lambda^{e \rightarrow d} = \{0\}, \quad (39)$$

$$g_t^{d_i} = \sigma(\tau_l^{d_{1,i}}(v_{l+1,t}^d) + \tau_l^{d_{2,i}}(h_{l,t}^e) + \tau_l^{d_{3,i}}(s_{l,t-1}^d)), \forall i \in \{1, 2, 3\}, \quad (40)$$

$$d_{l,t} = g_t^{d_1} \cdot \tau_l^{d_1}(v_{l+1,t}^d) + g_t^{d_2} \cdot \tau_l^{d_2}(h_{l,t}^e) + g_t^{d_3} \cdot \tau_l^{d_3}(s_{l,t-1}^d), \quad (41)$$

$$v_l^d = \rho_l^d(d_{l,t}), \quad (42)$$

$$h_l^e = d_{l,t}, \quad (43)$$

$$(44)$$

where the τ 's are affine transformations (for example a fully connected layer, a convolutional layer, or a transposed convolution layer), the ρ 's pointwise activation functions, σ a sigmoid activation function, and \cdot the element-wise multiplication.

2.4 Inference in a temporal model

In this section, we show that the same RLadder network can perform inference in temporal models. Consider a simple probabilistic model with three levels of hierarchy x_t, y_t, z_t in which variables vary in time (see Fig. 3a). The conditional distributions given the latent variables in the past y_{t-1}, z_{t-1}

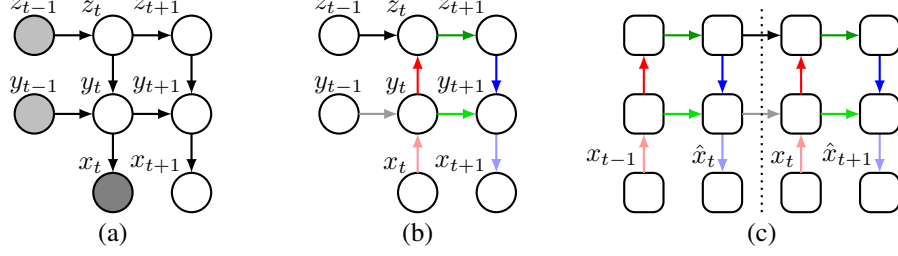


Figure 3: (a): Fragment of a graph of a temporal model relevant for updating the distributions of unknown variables after observing x_t . Light-gray circles represent latent variables whose distribution is not updated. (b): Directions of information propagation needed for inference. (c): The structure of the Ladder network can be seen as a computational graph implementing information flow in (b).

are defined as follows:

$$p(x_t|y_t) = N(x_t|w_x x_{t-1} + w_{xy} y_t, \sigma_x^2) \quad (45)$$

$$p(y_t|y_{t-1}, z_t) = N(y_t|w_y y_{t-1} + w_{yz} z_t, \sigma_y^2) \quad (46)$$

$$p(z_t|z_{t-1}) = N(z_t|w_z z_{t-1}, \sigma_z^2) \quad (47)$$

The part of the model graph that is relevant for updating the distributions of unknown variables given the observed sequence $x_{1..t-1} = (x_1, \dots, x_{t-1})$ and fixing the approximate distribution

$$\begin{aligned} p(y_{t-1}, z_{t-1}|x_{1..t-1}) &\approx q(y_{t-1})q(z_{t-1}) \\ q(y_{t-1}) &= N(y_{t-1}|m_{y,t-1}, v_{y,t-1}) \\ q(z_{t-1}) &= N(z_{t-1}|m_{z,t-1}, v_{z,t-1}) \end{aligned}$$

is shown in Fig. 3a.

Following the same logic as in Section 2.2, it is possible to show (see Appendix B) that in order to evaluate the approximate posterior distribution of the latent variables

$$p(y_t, z_t|x_{1..t}) \approx q(y_t)q(z_t) \quad (48)$$

$$q(y_t) = N(y_t|m_{y,t}, v_{y,t}) \quad (49)$$

$$q(z_t) = N(z_t|m_{z,t}, v_{z,t}), \quad (50)$$

one can first combine messages from the past (the expected outcome m') and from below (gray and red links in Fig. 3b) to get an update (\tilde{m}) based on the evidence (x):

$$\tilde{m}_{y,t} = s_{y,t} \frac{x_t}{w_{xy}} + (1 - s_{y,t}) m'_{y,t} \quad (51)$$

$$s_{y,t} = \text{sigmoid}(\log(\sigma_y^2 w_{xy}^2 / \sigma_x^2)) \quad (52)$$

$$\tilde{m}_{z,t} = s_{z,t} \frac{\tilde{m}_{y,t}}{w_{yz}} + (1 - s_{z,t}) m'_{z,t} \quad (53)$$

$$s_{z,t} = \text{sigmoid}(\log(\sigma_z^2 w_{yz}^2 / \sigma_y^2)) \quad (54)$$

$$(55)$$

and then combine the result with the latest approximation of the prior (green and blue lines) to get the updates posterior (m):

$$m_{z,t} = \tilde{m}_{z,t}, \quad (56)$$

$$m_{y,t} = \tilde{m}_{y,t} + \frac{w_{yz} v_{y,t}}{\sigma_y^2} (m_{z,t} - m'_{z,t}), \quad (57)$$

$$v_{y,t} = \left(\frac{w_x^2}{\sigma_x^2} + \frac{1}{\sigma_y^2} \right)^{-1}, \quad (58)$$

$$v_{z,t} = \left(\frac{w_{yz}^2}{\sigma_y^2} + \frac{1}{\sigma_z^2} \right)^{-1}. \quad (59)$$

At the same time as as the posterior is estimated, the expectation of the next time step (m') can also be estimated (also green and blue line):

$$m'_{z,t+1} = w_z m_{z,t}, \quad (60)$$

$$m'_{y,t+1} = w_y m_{y,t} + w_{yz} m'_{z,t+1}, \quad (61)$$

$$\hat{x}_{t+1} = w_x x_t + w_{xy} m'_{y,t+1}. \quad (62)$$

A computational graph which can implement those calculations is (using the notation of Eqns. (1)-(8)):

$$\Lambda^{d \rightarrow e} = \{0\}, \quad (63)$$

$$g_t^{e_i} = \sigma(\tau_l^{e_{1,i}}(v_{l-1,t}^e) + \tau_l^{e_{2,i}}(h_{l,t-1}^d) + \tau e_{3,i_l}(s_{l,t-1}^e)), \forall i \in \{1, 2, 3\}, \quad (64)$$

$$e_{l,t} = g_t^{e_1} \cdot \tau_l^{e_1}(v_{l-1,t}^e) + g_t^{e_2} \cdot \tau e_{2l}(h_{l,t-1}^d) + g_t^{e_3} \cdot \tau_l^{e_3}(s_{l,t-1}^e), \quad (65)$$

$$v_l^e = h_l^e = \rho_l^e(e_{l,t}), \quad (66)$$

$$\Lambda^{e \rightarrow d} = \{0\}, \quad (67)$$

$$g_t^{d_i} = \sigma(\tau_l^{d_{1,i}}(v_{l+1,t}^d) + \tau_l^{d_{2,i}}(h_{l,t}^e) + \tau_l^{d_{3,i}}(s_{l,t-1}^d) + \tau_l^{d_{4,i}}(h_{l+1,t-1}^d)), \forall i \in \{1, 2, 3, 4\}, \quad (68)$$

$$d_{l,t} = g_t^{d_1} \cdot \tau_l^{d_1}(v_{l+1,t}^d) + g_t^{d_2} \cdot \tau d_{2l}(h_{l,t}^e) + g_t^{d_3} \cdot \tau d_{3l}(s_{l,t-1}^d) + g_t^{d_4} \cdot \tau d_{4l}(h_{l+1,t-1}^d), \quad (69)$$

$$v_l^d = h_l^d = \rho_l^d(d_{l,t}), \quad (70)$$

where the τ 's are affine transformations (for example a fully connected layer, a convolutional layer, or a transposed convolution layer), the ρ 's point-wise activation functions, σ a sigmoid activation function, and \cdot the element-wise multiplication. But because the information about $h_{l+1,t-1}^d$ can be contained in $h_{l+1,t}^d$, $s_{l,t-1}^d$, and $h_{l+1,t}^d$, we can remove the dependency on $h_{l+1,t-1}^d$ in Eqns. 68 and 69 to get

$$g_t^{d_i} = \sigma(\tau_l^{d_{1,i}}(v_{l+1,t}^d) + \tau_l^{d_{2,i}}(h_{l,t}^e) + \tau_l^{d_{3,i}}(s_{l,t-1}^d)), \forall i \in \{1, 2, 3\}, \quad (71)$$

$$d_{l,t} = g_t^{d_1} \cdot \tau_l^{d_1}(v_{l+1,t}^d) + g_t^{d_2} \cdot \tau d_{2l}(h_{l,t}^e) + g_t^{d_3} \cdot \tau d_{3l}(s_{l,t-1}^d). \quad (72)$$

This computational graph is shown in Fig. 3c. Note that it has practically the same architecture as the graph for iterative inference in Fig. 2a. Using gatings in the bottom-up computations are justified by (51) and (53). Even though the top-down updates (57), (60), and (61) are simple summations in the case of this linear Gaussian model, the more general gatings in the top-down pass provides more flexibility for nonlinear models: The activations in the level above can select one of a few possible evolution scenarios on the level below. For these reasons we used standard LSTM and GRU cells as building blocks in RLadder.

As we discussed previously, Ladder networks are usually trained by introducing tasks that encourage the network to learn the optimal inference of the latent variables. For temporal models, the natural low-level task is predicting the input at the next time instance. Thus the cost is $-\log(p(x_{t+1}|x_{1..t}))$:

$$C_{\text{pred}} = (\hat{x}_{t+1} - x_{t+1})^2$$

where optimal \hat{x}_{t+1} is the expectation over $p(x_{t+1}|x_{1..t})$. The predictive distribution $p(x_{t+1}|x_{1..t})$ can be approximated with

$$p(x_{t+1}|x_{1..t}) \approx N(x_{t+1}|m'_{x,t+1}, v'_{x,t+1})$$

where $m'_{x,t+1} = w_x m'_{y,t+1}$ and the expression for $v'_{x,t+1}$ is given in Appendix B.

2.5 Modeling independent objects with RTagger

In many cognitive tasks, we need to model objects and their relations with each other. It can therefore be important to identify which parts of the sensory input belong to the same higher-level perceptual components (objects), a process called perceptual grouping. For example, if the task is to classify textured digits presented in the top row of Fig. 8, we need to separate them from a textured background. In this section, we explain the previously developed model for perceptual grouping called Tagger [12] and extend it to do inference with the proposed recurrent Ladder architecture. For another perspective

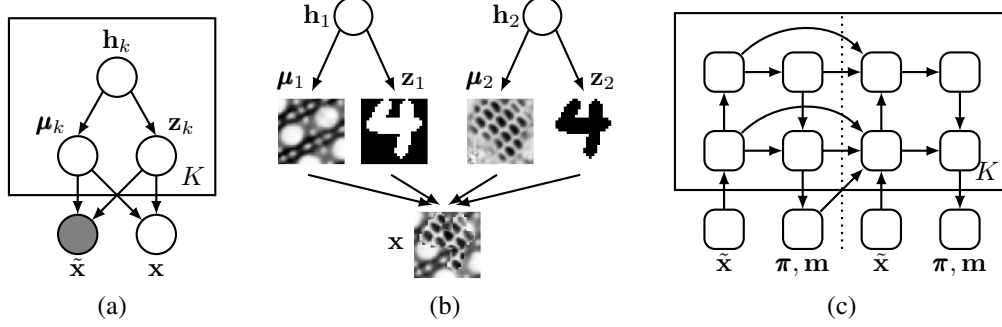


Figure 4: (a): Graphical model for perceptual grouping. (b): Examples of possible values of model variables for the textured MNIST dataset. (c): Computational graph that implements iterative inference in perceptual grouping task (RTagger). Two graph iterations are drawn.

on the problem see [13] which also extends Tagger to a recurrent neural network, but does so from an expectation maximization point of view.

Let us consider a probabilistic model that can be used to separate a textured object from a textured background. Each pixel x_i can belong to one of the K objects which is defined by binary variables $z_{i,k}$: $z_{i,k} = 1$ if pixel i belongs to object k and $z_{i,k} = 0$ otherwise. The look of object k is defined by variable \mathbf{m}_k which is a vector with as many elements $\mu_{i,k}$ as there are pixels. The joint probability distribution can be written as follows:

$$p(\mathbf{x}, \boldsymbol{\mu}, \mathbf{z}, \mathbf{h}) = \prod_{i,k} N(x_i | \mu_{i,k}, \sigma_k^2)^{z_{i,k}} \prod_{k=1}^K p(\mathbf{z}_k, \boldsymbol{\mu}_k | \mathbf{h}_k) p(\mathbf{h}_k) \quad (73)$$

where \mathbf{z}_k is a vector of elements $z_{i,k}$ and \mathbf{h}_k are latent variables which define the shape and the texture of the objects. See Fig. 4a for graphical representation of the model and Fig. 4b for possible values of model variables for the textured MNIST dataset.

To formulate the low-level training costs, we assume observing $\tilde{\mathbf{x}}$ which is a corrupted version of clean image \mathbf{x} :

$$p(\tilde{\mathbf{x}} | \mathbf{x}) = \prod_{i,k} N(\tilde{x}_i | x_i, \sigma^2).$$

Combining this with (73) and integrating out \mathbf{x} yields

$$p(\tilde{\mathbf{x}}, \boldsymbol{\mu}, \mathbf{z}, \mathbf{h}) = \prod_{i,k} N(\tilde{x}_i | \mu_{i,k}, \sigma_k^2 + \sigma^2)^{z_{i,k}} \prod_{k=1}^K p(\mathbf{z}_k, \boldsymbol{\mu}_k | \mathbf{h}_k) p(\mathbf{h}_k).$$

See also Fig. 4a for a graphical representation.

The inference procedure in this model should evaluate the posterior distributions of the latent variables $\mathbf{z}_k, \boldsymbol{\mu}_k, \mathbf{h}_k$ for each of the K groups given corrupted data $\tilde{\mathbf{x}}$. Making the approximation that the variables of each of the K groups are independent a posteriori

$$p(\mathbf{z}, \boldsymbol{\mu}, \mathbf{h} | \tilde{\mathbf{x}}) \approx q(\mathbf{z}, \boldsymbol{\mu}, \mathbf{h}) = \prod_k q(\mathbf{z}_k, \boldsymbol{\mu}_k, \mathbf{h}_k) = \prod_k q(\mathbf{z}_k, \boldsymbol{\mu}_k) q(\mathbf{h}_k),$$

the inference procedure can be implemented by updating each of the K distributions $q(\mathbf{z}_k, \boldsymbol{\mu}_k, \mathbf{h}_k)$ keeping the others fixed. For example, using the variational Bayesian approximation, the cost function

$$C_{\text{VB}} = \sum_k \langle \log q(\mathbf{z}_k, \boldsymbol{\mu}_k, \mathbf{h}_k) \rangle - \langle \log p(\tilde{\mathbf{x}} | \boldsymbol{\mu}_k, \mathbf{z}_k) \rangle - \langle \log p(\mathbf{z}_k, \boldsymbol{\mu}_k | \mathbf{h}_k) \rangle - \langle \log p(\mathbf{h}_k) \rangle \quad (74)$$

splits into a sum of terms corresponding to different groups and those terms can be optimized separately. Here $\langle \cdot \rangle$ denotes the expectation over $q(\mathbf{z}_k, \boldsymbol{\mu}_k, \mathbf{h}_k)$. Assuming that all the individual models $p(\mathbf{z}_k, \boldsymbol{\mu}_k, \mathbf{h}_k)$ have the same parametric form, the inference can be implemented using a computational graph with K copies of the same network doing inference for one of the groups. We use the RLadder architecture for doing individual inference, which gives the computational graph

presented in Fig. 4c.⁵ We refer to this model as RTagger, as it is a recurrent extension of the Tagger model [12].

As we stated earlier, understanding what kind of computations is needed in the inference procedure is crucial to come up with a good network architecture. For this reason, we derive quantities useful for updating the knowledge about latent variables \mathbf{z}_k and $\boldsymbol{\mu}_k$. Let us approximate the posterior distributions of those variables with

$$q(\mathbf{z}_k, \boldsymbol{\mu}_k) = \prod_i \pi_{i,k}^{z_{i,k}} N(\mu_{i,k} | m_{i,k}, v_{i,k}),$$

where $\pi_{i,k}$ is the posterior probability that pixel i belongs to object k and $m_{i,k}$ is the clean reconstruction of object k in pixel i . Keeping only terms in (74) dependent on m and π and ignoring the prior terms $p(\mathbf{z}_k, \boldsymbol{\mu}_k, \mathbf{h}_k)$ and $q(\mathbf{h}_k)$, because we are looking at messages needed in the bottom up pass, we are left with the first and the third terms of the cost function which are:

$$C_{\text{VB}}^* = \sum_k \langle \log q(\mathbf{z}_k, \boldsymbol{\mu}_k) - \log p(\tilde{\mathbf{x}} | \boldsymbol{\mu}_k, \mathbf{z}_k) \rangle. \quad (75)$$

Now taking the derivative of C_{VB}^* with respect to variational parameters $\pi_{i,k}$, $\mu_{i,k}$ yields (see Appendix C)

$$\frac{\partial C_{\text{VB}}^*}{\partial m_{i,k}} = \frac{\pi_{i,k}(m_{i,k} - \tilde{x}_{i,k})}{(\sigma_k^2 + \sigma^2)} \quad (76)$$

$$\frac{\partial C_{\text{VB}}^*}{\partial \pi_{i,k}} = \log \pi_{i,k} + 1 + \frac{1}{2} \log 2\pi(\sigma_k^2 + \sigma^2) + \frac{(\tilde{x}_{i,k} - m_{i,k})^2 + v_{k,i}}{2(\sigma_k^2 + \sigma^2)}. \quad (77)$$

Those are ‘messages’ useful to propagate from the corrupted observations $\tilde{\mathbf{x}}$ to update the knowledge about latent variables \mathbf{z}_k and $\boldsymbol{\mu}_k$.

Parameters $\pi_{i,k}$ and $m_{i,k}$ are computed from the activations at the bottom level at the end of every graph iteration (which corresponds to one bottom-up and one top-down pass). The variance parameters $v_{k,i}$ are not modeled explicitly and assumed zero in the computations. The values of $\pi_{i,k}$ and $m_{i,k}$, as well as the quantities in (76)–(77) are fed as inputs to the next graph iteration. For the first iteration, inputs $\pi_{i,k}$ and $m_{i,k}$ are set to random values. Note that corrupted data $\tilde{\mathbf{x}}$ are not fed to the network directly, only through the quantities in (76)–(77).

Learning the right inference procedure is encouraged by the low-level cost which is formulated using the clean data \mathbf{x} . The posterior distribution of clean data can be approximated with a mixture model:

$$\begin{aligned} p(x_i | \tilde{\mathbf{x}}) &= \sum_k \int p(x_i, z_{i,k} = 1, \mu_{i,k}, \mathbf{h}_k | \tilde{\mathbf{x}}) d\mu_{i,k} d\mathbf{h}_k \\ &= \sum_k \int p(x_i | z_{i,k} = 1, \mu_{i,k}) p(z_{i,k} = 1, \mu_{i,k} | \tilde{\mathbf{x}}) d\mu_{i,k} \\ &\approx \int p(x_i | z_{i,k} = 1, \mu_{i,k}) q(z_{i,k} = 1, \mu_{i,k}) d\mu_{i,k} \\ &= \sum_k q(z_{i,k} = 1) \int p(x_i | z_{i,k} = 1, \mu_{i,k}) q(\mu_{i,k}) d\mu_{i,k} \\ &= \sum_k \pi_{i,k} N(x_i | m_{i,k}, \sigma_k^2 + v_{i,k}). \end{aligned} \quad (78)$$

We use the negative logarithm of (78) as the training cost:

$$C_{\text{PG}} = -\log \sum_k \pi_{i,k} N(x_i | m_{i,k}, \sigma_k^2 + v_{i,k}). \quad (79)$$

Note that it is formulated in terms of parameters $\pi_{i,k}$, $m_{i,k}$ computed at the bottom layer at every iteration (see Fig. 4c).

⁵In principle, each of the K copies should be run keeping the others fixed for more stable convergence. However, we run the group updates in parallel to simplify implementation and speeding up the training process.

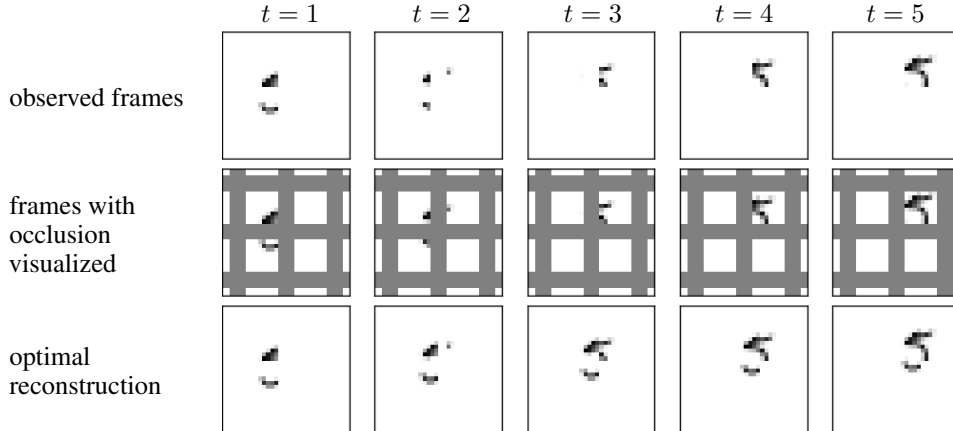


Figure 5: The Ocluded Moving MNIST data set. Bottom row: Optimal temporal recombination for a sequence of occluded frames from the dataset.

2.6 Related work

The proposed architecture is similar to that of other recently proposed models for temporal modeling [8, 9, 7, 6, 28]. In [7], the recurrent connections (from time $t - 1$ to time t) are placed in the lateral links between the encoder and the decoder. This can make it easier to extend an existing static architecture to the case of temporal modeling as the recurrent units do not participate in the bottom-up computations. On the other hand, the recurrent units do not receive information from the top, which makes it impossible for higher layers to influence the dynamics of lower layers. The architectures in [8, 9] are quite similar to ours but they could potentially derive further benefit from the decoder-to-encoder connections between successive time instances (grey and black links in Fig. 3c) for in their current state, the encoder cannot benefit from higher-level information. The aforementioned connections are well justified from the message-passing point of view: When updating the posterior distribution of a latent variable, one should combine the latest information from the top and from the bottom, and it is the decoder that contains the latest information from the top. We show empirical evidence to the importance of those connections in Section 3.1.

Iterative inference with neural architectures was previously proposed in deep Boltzmann machines [10], NADE-k [23] and recently for VAE [14]. Recurrent connections on high layers of Tagger network is also justified from Neural Expectation Maximization method [13] point of view. That architecture is simpler than Tagger and similarly performs perceptual grouping but uses recurrent neural networks (RNN) to model pixels and cluster assignments.

3 Experiments with temporal data

In this section, we demonstrate that the RLadder can learn an accurate inference algorithm in tasks that require temporal modeling. We demonstrate RLadder on two data sets in which passing information both in time and in abstraction hierarchy is important for achieving good performance, and in which multiple tasks on different abstraction levels can mutually benefit from each other.

3.1 Ocluded Moving MNIST

We use a dataset where we know how to do optimal inference in order to be able to compare the results of the RLadder to the optimal one. To this end we designed the Ocluded Moving MNIST dataset. It consists of MNIST digits downsampled to 14×14 pixels flying on a 32×32 white background with white vertical and horizontal occlusion bars (4 pixels in width, and spaced by 8 visible pixels apart) which, when the digit flies behind them, occludes the pixels of the digit (see Fig. 5). We also restrict the velocities to be randomly chosen in the set of 8 discrete velocities $\{(1, \pm 2), (-1, \pm 2), (2, \pm 1), (-2, \pm 1)\}$ pixels/frame, so that apart from the bouncing, the movement is deterministic. The digits are split into training, validation, and test sets according to the original

Table 1: Performance on Occluded Moving MNIST

	Classification error (%)	Prediction error, $\cdot 10^{-3}$
Optimal reconstruction and static classifier	0.71 ± 0.03	
Temporal baseline	2.02 ± 0.16	
Hierarchical RNN (encoder only)	1.60 ± 0.05	
RLadder w/o prediction task	1.51 ± 0.21	
RLadder w/o decoder-to-encoder conn.	1.24 ± 0.05	1.567 ± 0.004
RLadder w/o classification task		1.552 ± 0.025
RLadder	0.74 ± 0.09	1.501 ± 0.001

MNIST split. The primary task is then to classify the digit which is only partially observable at any given moment, at the end of five time steps.

In order to do optimal classification, one would need to assimilate information about the digit identity (which is only partially visible at any given time instance) by undoing the motion of the digit and superposing them by taking the maximum pixel value (see the bottom row of Fig. 5) and then feeding the resultant reconstruction to a classifier.

In order to encourage optimal inference we add a next step prediction task to the RLadder at the bottom of the decoder: The RLadder is trained to predict the next *occluded* frame, that is the network never sees the un-occluded digit. This thus mimics a realistic scenario where the ground truth is not known. To assess the importance of the features of the RLadder, we also evaluate its performance where we amputate some of its features individually. In addition we compare it to three other networks. In the first comparison network, the optimal reconstruction of the digit from the five frames (as shown in Fig. 5) is fed to a static feed-forward network from which the encoder of the RLadder was derived. This is our gold standard, and obtaining similar results to it implies doing close to optimal temporal inference. The second, a temporal baseline, is a deep feed-forward network (the one on which the encoder is based) with a recurrent neural network (RNN) at the top only so that, by design the network can propagate temporal information only at a high level, and not at a low level. The third, a hierarchical RNN, is the encoder only, the RLadder amputated of its decoder, is a stack of convolutional LSTM units with a few convolutional layers in between. See Fig. 6 for schematics of the architectures and Appendix D.1 for more details on the used architectures.

Fully supervised learning results

The results are presented in Table 1. The first thing to notice is that the RLadder reaches (up to uncertainty levels) the classification accuracy obtained by the network which was given the optimal reconstruction of the digit. Furthermore, if the RLadder does not have a decoder or the decoder-to-encoder connections, or if it is trained without the auxiliary prediction task, we see the classification error rise almost to the level of the temporal baseline. This means that even if a network has RNNs at the lowest levels (like with only the feed-forward encoder), or if it does not have a task which encourages it to develop a good world model (like the RLadder without the next-frame prediction task), or if the information cannot travel from the decoder to the encoder, the high level task cannot truly benefit from lower level temporal modeling.

Next, one notices from Table 1 that the top-level classification cost helps the low-level prediction cost in the RLadder (which in turn helps the top-level cost in a mutually beneficial cycle). This mutually supportive relationship between high-level and low-level inferences is nicely illustrated by the example in Fig. 7. Up until time step $t = 3$ inclusively, the network believes the digit to be a five (Fig. 7a). As such, at $t = 3$, the network predicts that the top right part of the five which has been occluded so far will stick out from behind the occlusions as the digit moves up and right at the next time step (Fig. 7b). Using the decoder-to-encoder connections, the decoder can relay this expectation to the encoder at $t = 4$. At $t = 4$ the encoder can compare this expectation with the actual input where the top right part of the five is absent (Fig. 7c). Without the decoder-to-encoder connections this comparison would have been impossible. Using the upward path of the encoder, the network can relay this discrepancy to the higher classification layers. These higher layers with a large receptive field can then conclude that since it is not a five, then it must be a three (Fig. 7d). Now thanks to the decoder, the higher classification layers can relay this information to the lower prediction layers so

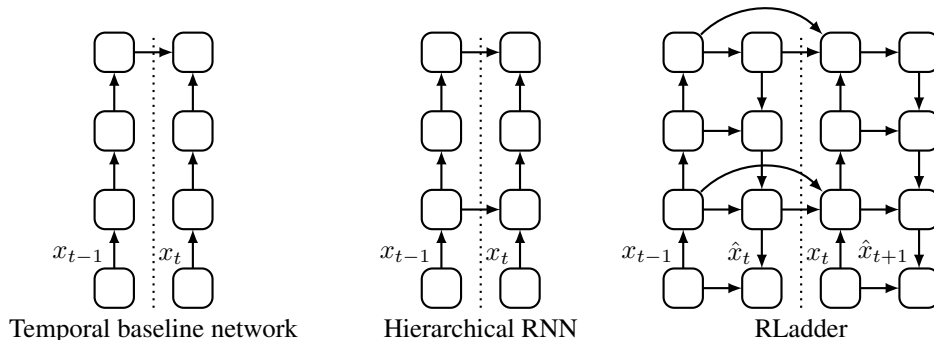


Figure 6: Architectures used for modeling occluded Moving MNIST. Temporal baseline network is a convolutional network with a fully connected RNN on top.

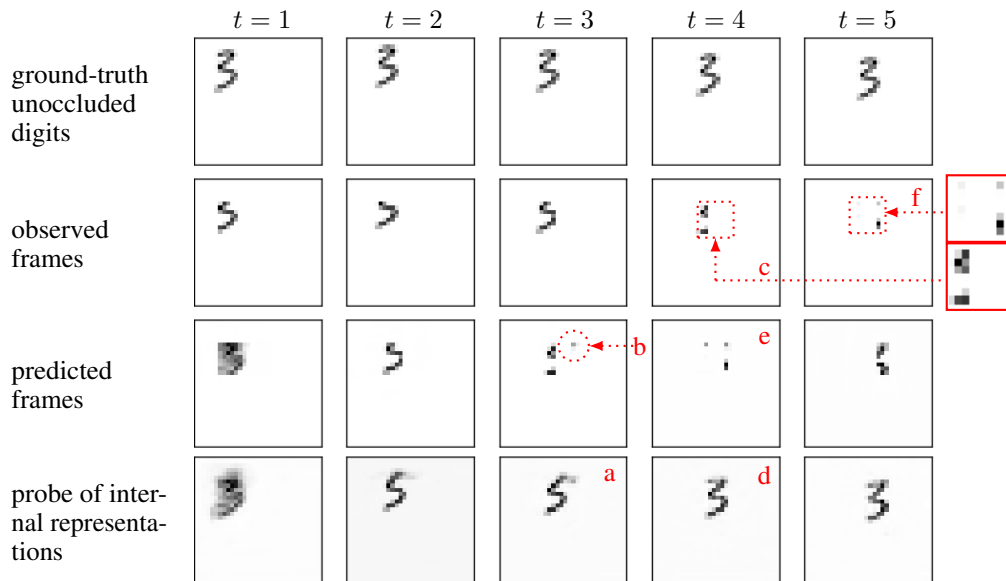


Figure 7: Example prediction of an RLadder on the occluded moving MNIST dataset. First row: the ground truth of the digit, which the network never sees and does not train on. Second row: The actual five frames seen by the network and on which it trains. Third row: the predicted next frames of a trained RLadder. Fourth row: A stopped-gradient (gradient does not flow into the RLadder) readout of the bottom layer of the decoder trained on the ground truth to probe what aspects of the digit are represented by the neurons which predict the next frame. Notice how at $t = 1$, the network does not yet know in which direction the digit will move and so it predicts a superposition of possible movements. Notice further (red annotations a-f), that until $t = 3$, the network thought the digit was a five, but when the top bar of the supposed five did not materialize on the other side of the occlusion as expected at $t = 4$, the network immediately concluded correctly that it was actually a three.

that they can change their prediction of what will be seen at $t = 5$ appropriately (Fig. 7e). Without a decoder which would bring this high level information back down to the low level, this drastic update of the prediction would be impossible. With this information the lower prediction layer can now predict that the top-left part of the three (which it has never seen before) will appear at the next time step from behind the occlusion, which is indeed what happens at $t = 5$ (Fig. 7f).

Semi-supervised learning results

A simple feed-forward network does not automatically take advantage of unlabeled data to improve performance on its task. As shown in Table 2 however, by adding 59k unlabeled occluded moving MNIST samples to the 1k labeled ones, an RLadder improves dramatically by learning a better model

Table 2: Classification error (%) on semi-supervised Occluded Moving MNIST

	1k labeled	1k labeled & 59k unlabeled	1k labeled & 59k unlabeled + WACT
Optimal reconstruction and static classifier	3.50 ± 0.28	3.50 ± 0.28	1.34 ± 0.04
Temporal baseline	10.86 ± 0.43	10.86 ± 0.43	3.14 ± 0.16
RLadder	10.49 ± 0.81	5.20 ± 0.77	1.69 ± 0.14

of the world. This is unlike the temporal baseline which cannot learn anything from the unlabeled samples without any additional mechanism.

There are other methods to make feed-forward networks take advantage of unlabeled data. One such method is weight-averaged consistency targets (WACT)[27] which is used to obtain state of the art results on semi-supervised classification of the SVHN dataset. But as the results in Table 2 show, RLadders can take advantage of this method too, in addition to its pre-existing performance boost due to unlabeled data.

3.2 Polyphonic Music Dataset

After a synthetic dataset with a high-level primary task, we think it good to evaluate an RLadder on a natural dataset with a low level primary task, on a totally different type of data. To this end, we chose the polyphonic music prediction/generation midi datasets converted to piano rolls and split into training, validation, and test set by Boulanger-Lewandowski *et al.* [4]. The dataset consists of piano rolls (the notes played at every time step, where a time step is, in this case, an eighth note) of various piano pieces. We train an 18-layer RLadder containing five convolutional LSTMs and one fully-connected LSTM. More details can be found in Appendix D.2.

Table 3: Negative log-likelihood (smaller is better) on polyphonic music dataset

	Piano-midi.de	Nottingham	Muse	JSB Chorales
Models outputting a joint distribution of notes:				
NADE masked [2]	7.42	3.32	6.48	8.51
NADE [2]	7.05	2.89	5.54	7.59
RNN-RBM [4]	7.09	2.39	6.01	6.27
RNN-NADE (HF) [4]	7.05	2.31	5.60	5.56
LSTM-NADE [15]	7.39	2.06	5.03	6.10
TP-LSTM-NADE [15]	5.49	1.64	4.34	5.92
BALSTM [15]	5.00	1.62	3.90	5.86
Models outputting marginal probabilities for each note:				
RNN [2]	7.88	3.87	7.43	8.76
LSTM [16]	6.866	3.492		
MUT1 [16]	6.792	3.254		
RLadder	6.19 ± 0.02	2.42 ± 0.03	5.69 ± 0.02	5.64 ± 0.02

Table 3 shows the negative log-likelihoods of the next-step prediction obtained on the music dataset, where our results are reported as mean plus or minus standard deviation over 10 seeds. We see that the RLadder is competitive with the best results, and give the best results amongst models outputting the marginal distribution of notes at each time step.

The fact that the RLadder did not beat [15] on the midi datasets shows one of the limitations of RLadder. Most the models in Table 3 output a joint probability distribution of notes, unlike RLadder which outputs the marginal probability for each note. That is to say, those models, to output the probability of a note, take as input the notes at previous time instances, but also the ground truth of the notes to the left at the same time instance. RLadder does not do that, it only takes as input the past notes played.

Even though, as the example in 3.1 of the the digit five turning into a three after seeing only one absent dot, shows that internally the RLadder models the joint distribution. One way Ladder could output a joint probability for the future state would be to output part of the distribution, then check the result, and based on that, iterate to the another part of the distribution. This brings us again to the iterative inference with the RLadder.

4 Experiments on perceptual grouping with RTagger

In this section, we show how the RTagger model described in Section 2.5 can be used to group pixels of the visual input into separate objects. First, we demonstrate this using a static image dataset where the clue for separating the objects from the background is the difference of the textures. Later, we apply essentially the same model to a temporal dataset where the clue for perceptual grouping is the difference of the object trajectories.

4.1 Grouping using texture information

The goal of the following experiment is to test the efficiency of the architecture proposed in Section 2.5 in grouping objects using the texture information. To this end, we created a dataset that contains thickened MNIST digits with the textures from the Brodatz dataset [5]. To create a greater diversity of textures (to avoid over-fitting), we randomly rotated and scaled the 20 available textures when producing the training data. Examples of the generated images are shown in the first row of Fig. 8.

The network trained on the textured MNIST dataset has the architecture presented in Fig. 4c with three iterations. The number of groups K was set to three. The details of the RLadder architecture which was trained to do inference for each of the K groups are presented in Appendix D.3. The network was trained on two tasks: The low-level segmentation task was formulated using the cost function (79). The top-level cost was the log-likelihood of the digit classes.

For comparison, we trained the Tagger model [12] on the same dataset. The Tagger architecture is similar to the one in Fig. 4c except that there are no connections on the higher levels between iterations. The only way the information propagates from the previous iteration to the next one is through the posterior group assignment probabilities $\pi_{i,k}$ and the clean image reconstructions $m_{i,k}$ at the bottom. Thus, the original Tagger network can not make use of the higher-level texture and object shape descriptors developed on the previous iteration and has to develop them again at every new iteration. The other comparison method was a feed-forward convolutional network which had an architecture resembling the bottom-up pass (encoder) of the RLadder. The network was trained on the classification task only.

Table 4 presents the obtained performance on the textured MNIST dataset in both fully supervised and semisupervised setting. Following [12], The segmentation accuracy was computed using the adjusted mutual information score [30] which is the mutual information between the ground truth segmentation and the estimated segmentation scaled to give 1 when the segmentations are identical and 0 when the output segmentation is random. Each pixel is assigned to the group which has the highest probability. Consistent with previous work [12, 11], we ignore the background in the case of a uniform 0-valued background and overlap regions when the overlap is ambiguous due to the shapes having the same colour and texture. The AMI score is computed as

$$s = \text{AMI}_{\max}(Z_T, Z_E) = \frac{I(Z_T, Z_E) - \langle I \rangle}{\max\{H(Z_T), H(Z_E)\} - \langle I \rangle},$$

where H is the entropy of a segmentation, Z_T is the ground truth segmentation, Z_E is the estimated segmentation (the maximum likelihood segmentation from Tagger), $I(Z_T, Z_E)$ is the mutual information between the two segmentations, and $\langle I \rangle$ is the average mutual information in all pairs of segmentations with up to R and C segments respectively.

The results obtained with the RTagger and Tagger clearly improve over iterations, which support the idea that iterative inference is useful for complex cognitive tasks. We also observe that RTagger outperforms Tagger as it can re-use the higher-level features developed on preceding iterations. Both approaches significantly outperform the convolutional network baseline in which the classification task is not supported by the input-level task.

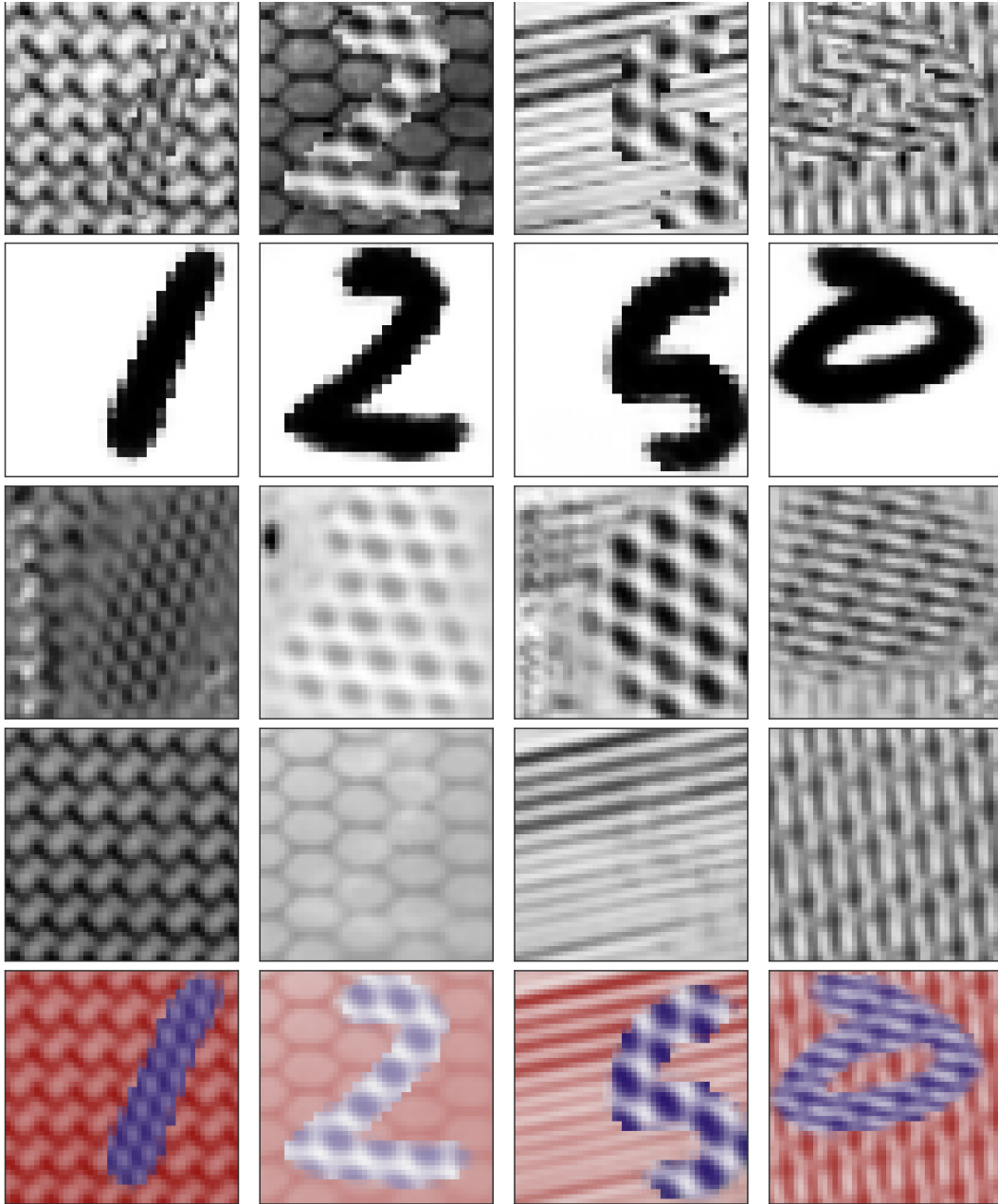


Figure 8: Row 1: Example images from the Brodatz-textured MNIST dataset. Row 2: Digit segmentation mask. Row 3: digit texture group reconstruction. Row 4: Background texture group reconstruction. Clearly, RTagger is able to fill in the missing textures for the digit and the background. In the last row, the segmented image is colored based on segmentation information.

To test whether the top-level classification task helps the low-level segmentation task, we trained the RTagger also without the classification task. Fig. 9 shows the progress of the segmentation accuracy during training for RTagger, RTagger without the classification cost and Tagger without the classification cost. One can observe that the top-level classification task helps to group pixels better on the input level. Thus, the high-level and low-level tasks mutually benefit from each other: Detecting object boundaries using textures helps to classify a digit, while knowing the class of the digit help to detect the object boundaries.

Table 4: Results on semisupervised classification task on Brodatz textured MNIST dataset over iterations i on fully supervised and semisupervised (1K labeled) case. Error rate of 1K labeled samples and 50K unlabeled samples show that RTagger is much more effective in combining multiple tasks. In fully labeled case, RTagger still achieves the best classification score comparing to the convnet. 50K unlabeled data is used in all cases except convnet.

		$i = 1$	$i = 2$	$i = 3$
1K labeled				
RTagger	Segmentation accuracy	0.56 ± 0.01	0.74 ± 0.03	0.80 ± 0.03
	Classification error, %	64.9 ± 17.0	29.2 ± 10.1	23.3 ± 6.3
Tagger	Segmentation accuracy	0.10 ± 0.09	0.19 ± 0.16	0.23 ± 0.18
	Classification error, %	56.0 ± 8.4	50.0 ± 8.1	49.3 ± 8.2
ConvNet [25]	Classification error, %	88 ± 0.30	–	–
50K labeled				
RTagger	Segmentation accuracy	0.55 ± 0.00	0.75 ± 0.02	0.80 ± 0.01
	Classification error, %	18.2 ± 1.6	8.0 ± 0.2	5.9 ± 0.2
Tagger	Segmentation accuracy	0.31 ± 0.20	0.45 ± 0.25	0.51 ± 0.25
	Classification error, %	26.5 ± 6.6	17.9 ± 8.4	17.13 ± 8.9
ConvNet [25]	Classification error, %	14.3 ± 0.46	–	–

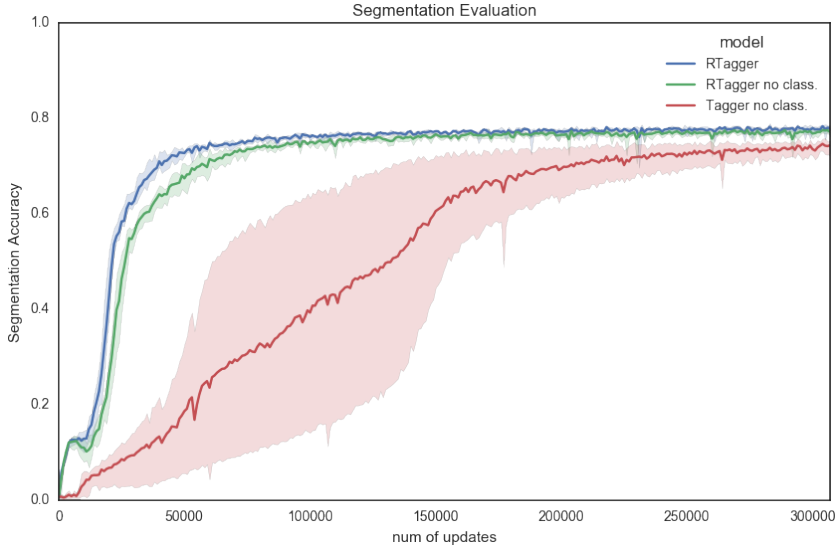


Figure 9: Progress of segmentation accuracy on validation set during training on the textured MNIST dataset. Solid line represents mean performance over 5 seeds and shades represents the fluctuations of segmentation performance over 5 seeds in [0, 100] percentile.

4.2 Grouping using higher level abstractions

The moving MNIST dataset [26]⁶ is one possible dataset to demonstrate one key shortcoming of the original Tagger which RTagger overcomes.

The easiest way to segment the digits correctly in the two digit moving MNIST is to segment them according to velocity. This is particularly true when the digits overlap. Velocity is not represented at the lowest level, where only pixels are represented. The original Tagger can only pass lowest level information to the next iteration, this makes it very difficult for it to segment according to higher level

⁶For this subsection, in order to have the ground truth segmentation, we reimplemented the dataset ourselves.

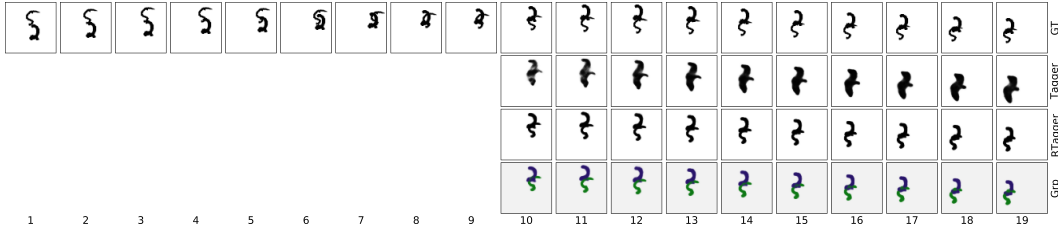


Figure 10: Moving MNIST segmentation and generation examples. From top to bottom, it’s the ground true moving sequence, generation by Tagger, generation by RTagger and segmentation by RTagger which is colored based on different groups. This hand picked example illustrates the failure mode of Tagger. RTagger makes it easy to group based on object velocities. The end result is that the generated sequence is much more realistic than what Tagger produces which completely mixes up the identity of the digits.

Table 5: Results on unsupervised moving MNIST segmentation task.

	Segmentation Accuracy
Tagger	0.52 ± 0.45
RTagger	0.75 ± 0.02

abstractions. Adding the higher level recurrences in RTagger, should allow it to develop and refine better higher level abstractions which can be used for segmentation.

To test this, we applied Tagger and RTagger to the moving MNIST dataset (see Table 5). As expected, RTagger consistently segmented the two digits correctly, while for two out of three seeds, Tagger failed to segment completely and when it did succeed, the segmentation was not as good. One of the interesting failure modes from Tagger is shown in Fig 10. Ground true frames is fed into step 0-9 and we conditionally generated next 10 step of the sequence. From this hand picked example we can see that, when Tagger fails to segment, it has difficulty generating sequences that has two digits overlap, while RTagger keeps digit identity during the generation. This is highly indicative that RTagger can better segment according to higher level abstractions than are available at the pixel level.

4.3 Next frame predictions in moving MNIST

To further compare our RLadder and RTagger models, and quantitatively compare the model modeling capacity, we trained our models on the well-established benchmark dataset moving MNIST [26]⁷. The goal of the experiment is to benchmark quantitatively how well our models can model video sequences. The final result is shown in Table 6. For each run, the model is trained in a stateful manner with 3 seed for 1.2 million updates. The test set is provided by the benchmark, hence the segmentation score was not computed. From the table, we can see that, with much less parameters, RLadder and RTagger is able to model close to video pixel network baseline. Interestingly, the difference between RLadder and RTagger is made because of the perceptual grouping mechanism in RTagger. Particularly, the best run from RTagger reaches 114 (nats/frame), which is very close to what VPN baseline is.

5 Conclusions

In the paper, we presented a recurrent extension of the Ladder network. The proposed architecture is motivated by the computations required in a hierarchical latent variable model. We empirically validated that the recurrent Ladder is able to learn accurate inference in challenging tasks which require modeling dependencies on multiple abstraction levels, iterative inference and temporal modeling. The proposed model outperformed strong baseline methods on two challenging classification tasks. It also produced competitive results on a temporal music data set. We envision that the proposed Recurrent Ladder will be a powerful building block for solving difficult cognitive tasks.

⁷http://www.cs.toronto.edu/~nitish/unsupervised_video

Table 6: Results on moving MNIST prediction task (nats/frame).

	Cross Entropy
Tagger	144.3 \pm 4.3
RLadder	128.4 \pm 0.1
RTagger	126.1 \pm 8.4
VPN Baseline [17]	110.1
VLN [7]	187.7

Acknowledgments

We would like to thank Klaus Greff and our colleagues from the Curious AI Company for their contribution in the presented work, specially Vikram Kamath and Matti Herranen.

References

- [1] Alain, G., Bengio, Y., and Rifai, S. (2012). Regularized auto-encoders estimate local statistics. *CoRR*, [abs/1211.4246](#).
- [2] Berglund, M., Raiko, T., Honkala, M., Kärkkäinen, L., Vetek, A., and Karhunen, J. T. (2015). Bidirectional recurrent neural networks as generative models. In *Advances in Neural Information Processing Systems*.
- [3] Bishop, C. M. (2006). *Pattern Recognition and Machine Learning (Information Science and Statistics)*. Springer-Verlag New York, Inc., Secaucus, NJ, USA.
- [4] Boulanger-Lewandowski, N., Bengio, Y., and Vincent, P. (2012). Modeling temporal dependencies in high-dimensional sequences: Application to polyphonic music generation and transcription. <http://arxiv.org/abs/1206.6392>.
- [5] Brodatz, P. (1966). *Textures: a photographic album for artists and designers*. Dover Pubns.
- [6] Canziani, A. and Culurciello, E. (2017). Cortexnet: a generic network family for robust visual temporal representations. <http://arxiv.org/abs/1706.02735>.
- [7] Cricri, F., Honkala, M., Ni, X., Aksu, E., and Gabbouj, M. (2016). Video Ladder networks. <http://arxiv.org/abs/1612.01756>.
- [8] Eyjolfsdottir, E., Branson, K., Yue, Y., and Perona, P. (2016). Learning recurrent representations for hierarchical behavior modeling. <http://arxiv.org/abs/1611.00094>.
- [9] Finn, C., Goodfellow, I. J., and Levine, S. (2016). Unsupervised learning for physical interaction through video prediction. In *Advances in Neural Information Processing Systems 29*.
- [10] Goodfellow, I., Mirza, M., Courville, A., and Bengio, Y. (2013). Multi-prediction deep Boltzmann machines. In *Advances in Neural Information Processing Systems*.
- [11] Greff, K., Srivastava, R. K., and Schmidhuber, J. (2015). Binding via reconstruction clustering. *CoRR*, [abs/1511.06418](#).
- [12] Greff, K., Rasmus, A., Berglund, M., Hao, T., Valpola, H., and Schmidhuber, J. (2016). Tagger: Deep unsupervised perceptual grouping. In *Advances in Neural Information Processing Systems 29*.
- [13] Greff, K., van Steenkiste, S., and Schmidhuber, J. (2017). Neural expectation maximization. In *ICLR Workshop*.
- [14] Hjelm, D., Salakhutdinov, R. R., Cho, K., Jovic, N., Calhoun, V., and Chung, J. (2016). Iterative refinement of the approximate posterior for directed belief networks. In *Advances in Neural Information Processing Systems*.
- [15] Johnson, D. D. (2017). Generating polyphonic music using tied parallel networks. In *International Conference on Evolutionary and Biologically Inspired Music and Art*.

- [16] Jozefowicz, R., Zaremba, W., and Sutskever, I. (2015). An empirical exploration of recurrent network architectures. In *Proceedings of the 32nd International Conference on Machine Learning (ICML-15)*.
- [17] Kalchbrenner, N., Oord, A. v. d., Simonyan, K., Danihelka, I., Vinyals, O., Graves, A., and Kavukcuoglu, K. (2016). Video pixel networks. *arXiv preprint arXiv:1610.00527*.
- [18] Kingma, D. and Ba, J. (2014). Adam: A method for stochastic optimization. <http://arxiv.org/abs/1412.6980>.
- [19] Kingma, D. P. and Welling, M. (2013). Auto-encoding variational Bayes. In *Proceedings of the 2nd International Conference on Learning Representations (ICLR)*.
- [20] Krizhevsky, A., Sutskever, I., and Hinton, G. E. (2012). Imagenet classification with deep convolutional neural networks. In *Advances in neural information processing systems*.
- [21] Neal, R. M. and Hinton, G. E. (1998). A view of the em algorithm that justifies incremental, sparse, and other variants. In *Learning in graphical models*, pages 355–368. Springer.
- [22] Raiko, T., Valpola, H., Harva, M., and Karhunen, J. (2007). Building blocks for variational Bayesian learning of latent variable models. *Journal of Machine Learning Research*, **8**(Jan), 155–201.
- [23] Raiko, T., Li, Y., Cho, K., and Bengio, Y. (2014). Iterative neural autoregressive distribution estimator NADE-k. In *Advances in neural information processing systems*.
- [24] Rasmus, A., Berglund, M., Honkala, M., Valpola, H., and Raiko, T. (2015). Semi-supervised learning with Ladder networks. In *Advances in Neural Information Processing Systems*.
- [25] Springenberg, J. T., Dosovitskiy, A., Brox, T., and Riedmiller, M. (2014). Striving for simplicity: The all convolutional net. *arXiv preprint arXiv:1412.6806*.
- [26] Srivastava, N., Mansimov, E., and Salakhudinov, R. (2015). Unsupervised learning of video representations using lstms. In *International Conference on Machine Learning*, pages 843–852.
- [27] Tarvainen, A. and Valpola, H. (2017). Weight-averaged consistency targets improve semi-supervised deep learning results. <http://arxiv.org/abs/1703.01780>.
- [28] Tietz, M., Alpay, T., Twiefel, J., and Wermter, S. (2017). Semi-supervised phoneme recognition with recurrent ladder networks. <http://arxiv.org/abs/1706.02124>.
- [29] Valpola, H. (2015). From neural PCA to deep unsupervised learning. *Advances in Independent Component Analysis and Learning Machines*.
- [30] Vinh, N. X., Epps, J., and Bailey, J. (2010). Information theoretic measures for clusterings comparison: Variants, properties, normalization and correction for chance. *Journal of Machine Learning Research*, **11**(Oct), 2837–2854.
- [31] Winn, J. and Bishop, C. M. (2005). Variational message passing. *Journal of Machine Learning Research*, **6**.

A Details on approximate inference in a simple static model

The model defined in Section 2.2 is:

$$\begin{aligned}
 p(\tilde{x}, x, y, z) &= p(z)p(y|z)p(x|y)p(\tilde{x}|x) \\
 p(z) &= N(z|\mu_z, \sigma_z^2) \\
 p(x|y) &= N(\tilde{x}|w_x y, \sigma_x^2) \\
 p(y|z) &= N(y|w_{yz} z, \sigma_y^2) \\
 p(\tilde{x}|y) &= N(\tilde{x}|x, \sigma^2)
 \end{aligned}$$

The cost function minimized in the variational Bayesian approach is:

$$C_{\text{VB}} = \langle \log q(x)q(y)q(z) \rangle - \langle \log p(\tilde{x}|x)p(x|y)p(y|z)p(z) \rangle ,$$

where the expectation is taken over $q(x, y, z)$. The first term of C_{VB} is

$$\begin{aligned}
 C_q &= \langle \log q(x)q(y)q(z) \rangle \\
 &= \left\langle -\frac{1}{2} \log 2\pi v_x - \frac{1}{2v_x} (x - m_x)^2 - \frac{1}{2} \log 2\pi v_y - \frac{1}{2v_y} (y - m_y)^2 - \frac{1}{2} \log 2\pi v_z - \frac{1}{2v_z} (z - m_z)^2 \right\rangle \\
 &= -\frac{1}{2} \log 2\pi v_x - \frac{1}{2} - \frac{1}{2} \log 2\pi v_y - \frac{1}{2} - \frac{1}{2} \log 2\pi v_z - \frac{1}{2} .
 \end{aligned}$$

The second term of C_{VB} is

$$\begin{aligned}
 C_p &= \langle \log p(\tilde{x}|x)p(x|y)p(y|z)p(z) \rangle \\
 &= \left\langle \frac{1}{2} \log 2\pi \sigma^2 + \frac{1}{2\sigma^2} (\tilde{x} - x)^2 + \frac{1}{2} \log 2\pi \sigma_x^2 + \frac{1}{2\sigma_x^2} (x - w_x y)^2 + \frac{1}{2} \log 2\pi \sigma_y^2 + \frac{1}{2\sigma_y^2} (y - w_{yz} z)^2 \right\rangle \\
 &\quad + \left\langle \frac{1}{2} \log 2\pi \sigma_z^2 + \frac{1}{2\sigma_z^2} (z - \mu_z)^2 \right\rangle \\
 &= \frac{1}{2} \log 2\pi \sigma^2 + \frac{1}{2\sigma^2} (\tilde{x}^2 - 2\tilde{x}m_x + m_x^2 + v_x) \\
 &\quad + \frac{1}{2} \log 2\pi \sigma_x^2 + \frac{1}{2\sigma_x^2} (m_x^2 + v_x - 2m_x w_x m_y + w_x^2 (m_y^2 + v_y)) \\
 &\quad + \frac{1}{2} \log 2\pi \sigma_z^2 + \frac{1}{2\sigma_z^2} (m_z^2 + v_z + \mu_z^2 - 2m_z \mu_z) \\
 &\quad + \frac{1}{2} \log 2\pi \sigma_y^2 + \frac{1}{2\sigma_y^2} (m_y^2 + v_y + w_{yz}^2 (m_z^2 + v_z) - 2m_y w_{yz} m_z) \\
 &= \frac{1}{2} \log 2\pi \sigma^2 + \frac{1}{2\sigma^2} ((\tilde{x} - m_x)^2 + v_x) + \frac{1}{2} \log 2\pi \sigma_x^2 + \frac{1}{2\sigma_x^2} ((m_x - w_x m_y)^2 + v_x + w_x^2 v_y) \\
 &\quad + \frac{1}{2} \log 2\pi \sigma_y^2 + \frac{1}{2\sigma_y^2} ((m_y - w_{yz} m_z)^2 + v_y + w_{yz}^2 v_z) + \frac{1}{2} \log 2\pi \sigma_z^2 + \frac{1}{2\sigma_z^2} ((m_z - \mu_z)^2 + v_z) .
 \end{aligned}$$

The derivatives of C_{VB} are:

$$\begin{aligned}
 \frac{\partial(C_q + C_p)}{\partial m_x} &= \frac{1}{\sigma^2} (m_x - \tilde{x}) + \frac{1}{\sigma_x^2} (m_x - w_x m_y) \\
 \frac{\partial(C_q + C_p)}{\partial v_x} &= -\frac{1}{2v_x} + \frac{1}{2\sigma^2} + \frac{1}{2\sigma_x^2} \\
 \frac{\partial(C_q + C_p)}{\partial m_y} &= \frac{w_x}{\sigma_x^2} (w_x m_y - m_x) + \frac{1}{\sigma_y^2} (m_y - w_{yz} m_z) \\
 \frac{\partial(C_q + C_p)}{\partial v_y} &= -\frac{1}{2v_y} + \frac{w_x^2}{2\sigma_x^2} + \frac{1}{2\sigma_y^2} \\
 \frac{\partial(C_q + C_p)}{\partial m_z} &= \frac{w_{yz}}{\sigma_y^2} (w_{yz} m_z - m_y) + \frac{1}{\sigma_z^2} (m_z - \mu_z) \\
 \frac{\partial(C_q + C_p)}{\partial v_z} &= -\frac{1}{2v_z} + \frac{w_{yz}^2}{2\sigma_y^2} + \frac{1}{2\sigma_z^2}
 \end{aligned}$$

Equating the derivatives to zeros and solving for the variational parameters gives:

$$\begin{aligned}
v_x &= \left(\frac{1}{\sigma^2} + \frac{1}{\sigma_x^2} \right)^{-1} \\
m_x &= v_x \left(\frac{\tilde{x}}{\sigma^2} + \frac{w_x m_y}{\sigma_x^2} \right) = s_x \tilde{x} + (1 - s_x) w_x m_y \\
s_x &= \text{sigmoid}(\log(\sigma_x^2 / \sigma^2)) \\
v_y &= \left(\frac{w_x^2}{\sigma_x^2} + \frac{1}{\sigma_y^2} \right)^{-1} \\
m_y &= v_y \left(\frac{m_x w_x}{\sigma_x^2} + \frac{w_{yz} m_z}{\sigma_y^2} \right) = s_y \frac{m_x}{w_x} + (1 - s_y) w_{yz} m_z \\
s_y &= \text{sigmoid}(\log(\sigma_y^2 w_x^2 / \sigma_x^2)) \\
v_z &= \left(\frac{w_{yz}^2}{\sigma_y^2} + \frac{1}{\sigma_z^2} \right)^{-1} \\
m_z &= v_z \left(\frac{m_y w_{yz}}{\sigma_y^2} + \frac{\mu_z}{\sigma_z^2} \right) = s_z \frac{m_y}{w_{yz}} + (1 - s_z) \mu_z \\
s_z &= \text{sigmoid}(\log(\sigma_z^2 w_{yz}^2 / \sigma_y^2)).
\end{aligned}$$

B Details on approximate inference in a simple temporal model

The simple temporal model defined in Section 2.4:

$$\begin{aligned}
p(x_t | y_t) &= N(x_t | w_x x_{t-1} + w_{xy} y_t, \sigma_x^2) \\
p(y_t | y_{t-1}, z_t) &= N(y_t | w_y y_{t-1} + w_{yz} z_t, \sigma_y^2) \\
p(z_t | z_{t-1}) &= N(z_t | w_z z_{t-1}, \sigma_z^2)
\end{aligned}$$

We assume that the distribution of y_{t-1} and z_{t-1} are fixed:

$$\begin{aligned}
p(y_{t-1} | x_{1..t-1}) &\approx q(y_{t-1}) = N(y_{t-1} | m_{y,t-1}, v_{y,t-1}) \\
p(z_{t-1} | x_{1..t-1}) &\approx q(z_{t-1}) = N(z_{t-1} | m_{z,t-1}, v_{z,t-1}).
\end{aligned}$$

We approximate the posterior distributions of y_t, z_t

$$\begin{aligned}
p(y_t, z_t | x_{1..t}) &\approx q(y_t) q(z_t) \\
q(y_t) &= N(y_t | m_{y,t}, v_{y,t}) \\
q(z_t) &= N(z_t | m_{z,t}, v_{z,t}),
\end{aligned} \tag{80}$$

The cost function minimized in the variational Bayesian approach is:

$$C_{\text{VB}} = \langle \log q(y_t) q(z_t) - \log p(x_t | y_t) p(y_t | y_{t-1}, z_t) p(z_t | z_{t-1}) - \log p(y_{t-1}) p(z_{t-1}) \rangle$$

where the expectation is taken over $q(y_t, z_t, y_{t-1}, z_{t-1}, \dots, y_1, z_1) = \prod_{s=1}^t q(y_s) q(z_s)$. Let us elaborate the terms of C_{VB} . The first term is

$$\begin{aligned}
C_q &= \left\langle -\frac{1}{2} \log 2\pi v_{y,t} - \frac{1}{2v_{y,t}} (y_t - m_{y,t})^2 - \frac{1}{2} \log 2\pi v_{z,t} - \frac{1}{2v_{z,t}} (z_t - m_{z,t})^2 \right\rangle \\
&= -\frac{1}{2} \log 2\pi v_{y,t} - \frac{1}{2} - \frac{1}{2} \log 2\pi v_{z,t} - \frac{1}{2}.
\end{aligned}$$

The second term is

$$\begin{aligned}
C_p &= - \left\langle -\frac{1}{2} \log 2\pi \sigma_x^2 - \frac{1}{2\sigma_x^2} (x_t - w_x y_t)^2 - \frac{1}{2} \log 2\pi \sigma_y^2 - \frac{1}{2\sigma_y^2} (y_t - w_y y_{t-1} - w_{yz} z_t)^2 \right\rangle \\
&\quad - \left\langle -\frac{1}{2} \log 2\pi \sigma_z^2 - \frac{1}{2\sigma_z^2} (z_t - w_z z_{t-1})^2 \right\rangle \\
&= \frac{1}{2} \log 2\pi \sigma_x^2 + \frac{1}{2\sigma_x^2} (x_t^2 - 2x_t w_x m_{y,t} + w_x^2 (m_{y,t}^2 + v_{y,t})) \\
&\quad + \frac{1}{2} \log 2\pi \sigma_y^2 + \frac{1}{2\sigma_y^2} (m_{y,t}^2 + v_{y,t} + w_y^2 (m_{y,t-1}^2 + v_{y,t-1}) + w_{yz}^2 (m_{z,t}^2 + v_{z,t}) \\
&\quad - 2m_{y,t} w_y m_{y,t-1} - 2m_{y,t} w_{yz} m_{z,t} + 2w_y m_{y,t-1} w_{yz} m_{z,t}) \\
&\quad + \frac{1}{2} \log 2\pi \sigma_z^2 + \frac{1}{2\sigma_z^2} (m_{z,t}^2 + v_{z,t} - 2m_{z,t} w_z m_{z,t-1} + w_z^2 (m_{z,t-1}^2 + v_{z,t-1})).
\end{aligned}$$

The last term is a function of variational parameters $m_{y,t-1}, m_{z,t-1}, v_{y,t-1}, v_{z,t-1}$ which we do not update at time instance t . Taking the derivative of C_{VB} wrt the variational parameters yields:

$$\begin{aligned}\frac{\partial C_{\text{VB}}}{\partial m_{y,t}} &= \frac{1}{\sigma_x^2}(-x_t w_x + w_x^2 m_{y,t}) + \frac{1}{\sigma_y^2}(m_{y,t} - w_y m_{y,t-1} - w_{yz} m_{z,t}) \\ \frac{\partial C_{\text{VB}}}{\partial v_{y,t}} &= -\frac{1}{2v_{y,t}} + \frac{w_x^2}{2\sigma_x^2} + \frac{1}{2\sigma_y^2} \\ \frac{\partial C_{\text{VB}}}{\partial m_{z,t}} &= \frac{w_{yz}}{\sigma_y^2}(w_{yz} m_{z,t} - m_{y,t} + w_y m_{y,t-1}) + \frac{1}{\sigma_z^2}(m_{z,t} - w_z m_{z,t-1}) \\ \frac{\partial C_{\text{VB}}}{\partial v_{z,t}} &= -\frac{1}{2v_{z,t}} + \frac{w_{yz}^2}{2\sigma_y^2} + \frac{1}{2\sigma_z^2}.\end{aligned}$$

Equating the derivatives to zero yields:

$$\begin{aligned}v_{y,t} &= \left(\frac{w_x^2}{\sigma_x^2} + \frac{1}{\sigma_y^2}\right)^{-1} \\ m_{y,t} &= v_{y,t} \left(\frac{x_t w_x}{\sigma_x^2} + \frac{w_y m_{y,t-1} + w_{yz} m_{z,t}}{\sigma_y^2}\right) \\ v_{z,t} &= \left(\frac{w_{yz}^2}{\sigma_y^2} + \frac{1}{\sigma_z^2}\right)^{-1} \\ m_{z,t} &= v_{z,t} \left(\frac{(m_{y,t} - w_y m_{y,t-1}) w_{yz}}{\sigma_y^2} + \frac{w_z m_{z,t-1}}{\sigma_z^2}\right).\end{aligned}$$

These computations can be done by first estimating $m_{y,t}, m_{z,t}$ before observing x_t and then correcting using the observation. Let us show how it is done for $m_{y,t}$. We define $m'_{y,t}$ to be the posterior mean before observing x_t (next step decoder prediction), $\tilde{m}_{y,t}$ (encoder posterior) to be the posterior means after observing x_t but before updating the approximate posterior of higher latent variables (z in this case), and finally $m_{y,t}$ to be the posterior mean after observing x_t and updating all posteriors (decoder, same step prediction). Thus, we can write

$$m'_{y,t} = w_y m_{y,t-1} + w_{yz} m'_{z,t} \quad (81)$$

$$\tilde{m}_{y,t} = v_{y,t} \left(\frac{x_t w_x}{\sigma_x^2} + \frac{m'_{y,t}}{\sigma_y^2}\right) = s_{y,t} \frac{x_t}{w_x} + (1 - s_{y,t}) m'_{y,t} \quad (82)$$

$$s_{y,t} = \text{sigmoid}(\log(\sigma_y^2 w_x^2 / \sigma_x^2)) \quad (83)$$

$$m_{y,t} = \tilde{m}_{y,t} + \frac{w_{yz} v_{y,t}}{\sigma_y^2} (m_{z,t} - m'_{z,t}), \quad (84)$$

which if we eliminate the tilded and primed m 's, give exactly the same equations as previously.

For a generic level l in a hierarchical chain, we have:

$$m'_{l,t} = w_l m_{l,t-1} + w_{l,l+1} m'_{l+1,t} \quad (85)$$

$$\tilde{m}_{l,t} = m'_{l,t} + \frac{(1 - s_l)}{w_{l-1,l}} (\tilde{m}_{l-1,t} - m'_{l-1,t}) \quad (86)$$

$$s_l = \frac{\frac{1}{\sigma_l^2}}{\frac{1}{\sigma_l^2} + \frac{w_{l-1,l}^2}{\sigma_{l-1}^2}} = \text{sigmoid}(\log(\sigma_l^2 w_{l-1,l}^2 / \sigma_{l-1}^2)) \quad (87)$$

$$m_{l,t} = \tilde{m}_{l,t} + s_l w_{l,l+1} (m_{l+1,t} - m'_{l+1,t}) \quad (88)$$

C Details on model for perceptual grouping

Consider the model defined in Section 2.5. Each element x_i of the input vector can belong to one of the K objects. $z_{i,k}$ is a binary random variable which identifies to which object element x_i belongs: $z_{i,k} = 1$ if x_i belongs to object k and $z_{i,k} = 0$ otherwise. Variable $\boldsymbol{\mu}_k$ is the reconstruction of object k defined for all pixels. The joint probability distribution is:

$$p(\mathbf{x}, \boldsymbol{\mu}, \mathbf{z}, \mathbf{h}) = \prod_{i,k} N(x_i | \mu_{i,k}, \sigma_k^2)^{z_{i,k}} \prod_{k=1}^K p(\mathbf{z}_k, \boldsymbol{\mu}_k | \mathbf{h}_k) p(\mathbf{h}_k)$$

where \mathbf{z}_k is a vector of elements $z_{i,k}$ and \mathbf{h}_k are latent variables which define the shape and the texture of the objects. We observe noisy version $\tilde{\mathbf{x}}$ of the clean inputs \mathbf{x} :

$$p(\tilde{\mathbf{x}} | \mathbf{x}) = \prod_{i,k} N(\tilde{x}_i | x_i, \sigma^2).$$

Combining this with $p(\mathbf{x}, \boldsymbol{\mu}, \mathbf{z}, \mathbf{h})$ and integrating out \mathbf{x} yields

$$p(\tilde{\mathbf{x}}|\boldsymbol{\mu}, \mathbf{z}) = \prod_{i,k} N(\tilde{x}_i|\mu_{i,k}, \sigma_k^2 + \sigma^2)^{z_{i,k}}$$

$$p(\tilde{\mathbf{x}}, \boldsymbol{\mu}, \mathbf{z}, \mathbf{h}) = \prod_{i,k} N(\tilde{x}_i|\mu_{i,k}, \sigma_k^2 + \sigma^2)^{z_{i,k}} \prod_{k=1}^K p(\mathbf{z}_k, \boldsymbol{\mu}_k|\mathbf{h}_k)p(\mathbf{h}_k).$$

We approximate the true posterior distribution with

$$p(\mathbf{z}, \boldsymbol{\mu}, \mathbf{h}|\tilde{\mathbf{x}}) \approx q(\mathbf{z}, \boldsymbol{\mu}, \mathbf{h}) = \prod_k q(\mathbf{z}_k)q(\boldsymbol{\mu}_k)q(\mathbf{h}_k)$$

where

$$q(\mathbf{z}_k) = \prod_{i,k} \pi_{i,k}^{z_{i,k}}$$

is a categorical distribution and $\pi_{i,k}$ is the posterior probability that x_i belongs to group k . $q(\boldsymbol{\mu})$ is a Gaussian distribution with independent elements $\mu_{i,k}$:

$$q(\boldsymbol{\mu}_k) = \prod_{i,k} N(\mu_{i,k}|m_{i,k}, v_{i,k}).$$

Using the variational Bayes approach, we can write the cost function to be minimized:

$$C_{\text{VB}} = \sum_k \langle \log q(\mathbf{z}_k, \boldsymbol{\mu}_k) + \log q(\mathbf{h}_k) - \log p(\tilde{\mathbf{x}}|\boldsymbol{\mu}_k, \mathbf{z}_k) - \log p(\mathbf{z}_k, \boldsymbol{\mu}_k|\mathbf{h}_k) - \log p(\mathbf{h}_k) \rangle \quad (89)$$

where the expectation is taken over $q(\mathbf{z}, \boldsymbol{\mu}, \mathbf{h})$. Keeping only terms dependent on m and π and ignoring the prior terms $p(\mathbf{z}_k, \boldsymbol{\mu}_k, \mathbf{h}_k)$ and $q(\mathbf{h}_k)$, because we are looking at messages needed in the bottom up pass, we are left with the first and the third terms of the cost function which are:

$$C_{\text{VB}}^* = \left\langle \sum_{i,k} z_{i,k} \log \pi_{i,k} - \frac{1}{2} \log 2\pi v_{i,k} - \frac{(\mu_{i,k} - m_{i,k})^2}{2v_{i,k}} \right\rangle$$

$$- \left\langle - \sum_{i,k} \frac{z_{i,k}}{2} \log 2\pi(\sigma_k^2 + \sigma^2) + \frac{z_{i,k}(\tilde{x}_{i,k} - \mu_{i,k})^2}{2(\sigma_k^2 + \sigma^2)} \right\rangle$$

$$= \sum_{i,k} \pi_{i,k} \log \pi_{i,k} - \frac{1}{2} \log 2\pi v_{i,k} - \frac{1}{2}$$

$$+ \sum_{i,k} \frac{\pi_{i,k}}{2} \log 2\pi(\sigma_k^2 + \sigma^2) + \frac{\pi_{i,k}((\tilde{x}_{i,k} - m_{i,k})^2 + v_{i,k})}{2(\sigma_k^2 + \sigma^2)}.$$

The derivatives of C_{VB}^* are:

$$\frac{\partial C_{\text{VB}}^*}{\partial m_{i,k}} = \frac{\pi_{i,k}(m_{i,k} - \tilde{x}_{i,k})}{(\sigma_k^2 + \sigma^2)}$$

$$\frac{\partial C_{\text{VB}}^*}{\partial \pi_{i,k}} = \log \pi_{i,k} + 1 + \frac{1}{2} \log 2\pi(\sigma_k^2 + \sigma^2) + \frac{(\tilde{x}_{i,k} - m_{i,k})^2 + v_{i,k}}{2(\sigma_k^2 + \sigma^2)}.$$

The conditional distribution of the clean data given the corrupted data:

$$p(x_i|\tilde{\mathbf{x}}) = \sum_k \int p(x_i, z_{i,k} = 1, \mu_{i,k}, \mathbf{h}_k|\tilde{\mathbf{x}})d\mu_{i,k}d\mathbf{h}$$

$$= \sum_k \int p(x_i|z_{i,k} = 1, \mu_{i,k})p(z_{i,k} = 1, \mu_{i,k}|\tilde{\mathbf{x}})d\mu_{i,k}$$

$$\approx \sum_k \int p(x_i|z_{i,k} = 1, \mu_{i,k})q(z_{i,k} = 1)q(\mu_{i,k})d\mu_{i,k}$$

$$= \sum_k \pi_{i,k} \int N(\tilde{x}_i|\mu_{i,k}, \sigma_k^2)N(\mu_{i,k}|m_{i,k}, v_{i,k})d\mu_{i,k}$$

$$= \sum_k \pi_{i,k} N(x_i|m_{i,k}, \sigma_k^2 + v_{i,k}).$$

D Details of experiments

The following cells were used in the decoder of the RLadder. G1 cell receives vector \mathbf{x}_{top} from the top and vector \mathbf{x}_{lat} from the lateral connection and passes \mathbf{y} to the level below:

$$\begin{aligned}\mathbf{u} &= \mathbf{A}\mathbf{x}_{\text{top}} + \mathbf{b} \\ \boldsymbol{\mu} &= f(\mathbf{u}, \mathbf{w}_1) \\ \mathbf{s} &= f(\mathbf{u}, \mathbf{w}_2) \\ \mathbf{y} &= \mathbf{x}_{\text{lat}}\mathbf{s} + (1 - \mathbf{s})\boldsymbol{\mu},\end{aligned}$$

where

$$f(\mathbf{u}, \mathbf{w}) = w_0 \text{sigmoid}(w_1 \mathbf{u} + w_2) + w_3 \mathbf{u} + w_4$$

with w_i being the elements of vector \mathbf{w} . In the convolutional version ConvG1 of that cell, \mathbf{u} in the first formula is computed with convolution

$$\mathbf{u} = \mathbf{A} * \mathbf{x}_{\text{top}} + \mathbf{b}.$$

ConvG2 cell also receives \mathbf{x}_{top} , \mathbf{x}_{lat} and outputs \mathbf{y} :

$$\begin{aligned}\boldsymbol{\mu}_1 &= f(\mathbf{A}_1 * \mathbf{x}_{\text{top}} + \mathbf{B}_1 * \mathbf{x}_{\text{lat}} + \mathbf{b}_1, \mathbf{w}_1) \\ \boldsymbol{\mu}_2 &= f(\mathbf{A}_2 * \mathbf{x}_{\text{top}} + \mathbf{B}_2 * \mathbf{x}_{\text{lat}} + \mathbf{b}_2, \mathbf{w}_2) \\ \mathbf{s} &= f(\mathbf{A}_s * \mathbf{x}_{\text{top}} + \mathbf{B}_s * \mathbf{x}_{\text{lat}} + \mathbf{b}_s, \mathbf{w}_s) \\ \mathbf{y} &= \boldsymbol{\mu}_1 \mathbf{s} + (1 - \mathbf{s})\boldsymbol{\mu}_2\end{aligned}$$

The computations in the ConvG3 cell are performed as follows:

$$\begin{aligned}\mathbf{u} &= \text{relu}(\mathbf{A}_1 * \mathbf{x}_{\text{top}} + \mathbf{B}_1 * \mathbf{x}_{\text{lat}} + \mathbf{b}_1, \mathbf{w}_1) \\ \boldsymbol{\mu}_1 &= \mathbf{W}_1 * \mathbf{u} \\ \boldsymbol{\mu}_2 &= \mathbf{W}_2 * \mathbf{u} \\ \mathbf{s} &= \text{sigmoid}(\mathbf{W}_s * \mathbf{u}) \\ \mathbf{y} &= \boldsymbol{\mu}_1 \mathbf{s} + (1 - \mathbf{s})\boldsymbol{\mu}_2.\end{aligned}$$

D.1 Details of experiments with Occluded Moving MNIST

The RLadder architecture trained for the occluded moving MNIST dataset is presented in Table 7. The architecture of the baseline temporal model and the static feed-forward network trained on optimal digit reconstructions are shown in Figs. 8–9.

We trained using the Adam optimizer [18] with an initial learning rate of 0.001, only on the training set. But every time the classification error on the validation set rises, we divided the learning rate by 2 until a minimum value of 0.0001. We then never trained the network on the validation set, we simply evaluated it on the test set as trained on the training set.

D.2 Details of experiments with Polyphonic Music data

The RLadder architecture trained for the music dataset is presented in Table 10. For the Midi dataset, we trained using the Adam optimizer with a learning rate of 0.01. Because the network overfitted very rapidly, we determined the optimal stopping time using the validation set and then trained on the training and validation set for the same number of epochs (between 3 and 10 depending on the hyperparameters).

D.3 Details of experiments with textured MNIST

The RTagger architecture used to train on Brodatz-textured MNIST data is in Table 11. For the baseline model, The baseline model for texture MNIST is from the model C in Springenberg *et al.* [25].

The networks were trained using the Adam optimizer with learning rate 0.0004. All training results were evaluated at update 160000. The size of the image batch was 16 for all models. Batch normalization was applied to encoder and decoder layers.

Table 7: Structure of RLadder for occluded moving MNIST

Encoder				Decoder	
Layer	Stride	# channels (size)	filter size		filter size
Input	-	1			
ConvLSTM	1	32	(3, 3)	convG3	(9,9)
Conv	1	32	(3, 3)	convG3	(3, 3)
Conv	1	32	(3, 3)	convG3	(3, 3)
Conv	1	32	(3, 3)	convG3	(3, 3)
Pool	2	MAX	(2, 2)	convG3	(6, 6)
ConvLSTM	1	32	(3, 3)	convG3	(9, 9)
Conv	1	64	(3, 3)	convG3	(3, 3)
Conv	1	64	(3, 3)	convG3	(3, 3)
Conv	1	64	(3, 3)	convG3	(3, 3)
Pool	2	MAX	(2, 2)	convG3	(6, 6)
Conv	1	128	(3, 3)	convG3	(3, 3)
Conv	1	64	(1, 1)	convG3	(3, 3)
Conv	1	32	(1, 1)	convG3	(3, 3)
Pool	2	AVG	(2, 2)	G1	
LSTM		16		G1	
SoftMax		10		-	

Table 8: Temporal baseline network for occluded moving MNIST

Layer	Stride	# channels (size)	filter size
Input	-	1	
Conv	1	32	(3, 3)
Conv	1	32	(3, 3)
Conv	1	32	(3, 3)
Pool	2	MAX	(2, 2)
Conv	1	64	(3, 3)
Conv	1	64	(3, 3)
Conv	1	64	(3, 3)
Pool	2	MAX	(2, 2)
Conv	1	128	(3, 3)
Conv	1	64	(1, 1)
Conv	1	32	(1, 1)
Pool	2	AVG	(2, 2)
LSTM		16	
SoftMax		10	

Table 9: Feed-forward network in which the optimal temporal reconstruction of occluded moving MNIST is inputted for classification

Layer	Stride	# channels (size)	filter size
Input	-	1	
Conv	1	32	(3, 3)
Conv	1	32	(3, 3)
Conv	1	32	(3, 3)
Pool	2	MAX	(2, 2)
Conv	1	64	(3, 3)
Conv	1	64	(3, 3)
Conv	1	64	(3, 3)
Pool	2	MAX	(2, 2)
Conv	1	128	(3, 3)
Conv	1	64	(1, 1)
Conv	1	32	(1, 1)
Pool	2	AVG	(2, 2)
SoftMax		10	

Table 10: Structure of RLadder for Polyphonic Music dataset

Layer	Encoder			Decoder	
	Stride	# channels (size)	filter size		filter size
Input	-	1			
ConvLSTM	1	32	(1, 3)	ConvG2	(1,3)
ConvLSTM	2	64	(1, 3)	ConvG2	(1,3)
ConvLSTM	2	96	(1, 3)	ConvG2	(1,3)
ConvLSTM	2	128	(1, 3)	ConvG2	(1,3)
ConvLSTM	2	160	(1, 3)	ConvG2	(1,3)
Pool	2	AVG	(1, 2)	G1	
LSTM		96		G1	
SoftMax		19		Identity	

Table 11: Structure of RTagger for textured MNIST dataset

Layer	Encoder			Decoder	
	Stride	# channels (size)	filter size		
Input	-	1			
ConvLSTM	2	96	(8, 8)	ConvG1	
Conv	1	96	(5, 5)	ConvG1	
Conv	1	96	(5, 5)	ConvG1	
ConvLSTM	2	192	(4, 4)	ConvG1	
Conv	1	192	(5, 5)	ConvG1	
Conv	1	192	(5, 5)	ConvG1	
ConvLSTM	2	192	(4, 4)	ConvG1	
Conv	1	192	(5, 5)	ConvG1	
Conv	1	192	(5, 5)	ConvG1	
ConvLSTM	2	11	(4, 4)	ConvG1	
Pool	-	-	(6,6)	AVERAGE	
FC	-	11	-	G1	